

1 QBOi El Niño Southern Oscillation experiments: Assessing 2 relationships between ENSO, MJO, and QBO

3 Dillon Elsbury^{1,2}, Federico Serva³, Julie M. Caron⁴, Seung-Yoon Back⁵, Clara Orbe⁶, Jadwiga H. Richter⁴
4 James A. Anstey⁷, Neal Butchart⁸, Chih-Chieh Chen⁴, Javier García-Serrano^{9,10}, Anne Glanville⁴, Yoshio
5 Kawatani^{11,12}, Tobias Kerzenmacher¹³, Francois Lott¹⁴, Hiroaki Naoe¹⁵, Scott Osprey^{16,17}, Froila M.
6 Palmeiro^{9,18}, Seok-Woo Son⁵, Masakazu Taguchi¹⁹, Stefan Versick¹³, Shingo Watanabe²⁰, Kohei
7 Yoshida¹⁵

8
9 ¹ Cooperative Institute for Research in Environmental Sciences University of Colorado Boulder, Boulder, Colorado, USA

10
11 ² NOAA/Chemical Sciences Laboratory, Boulder, Colorado, USA

12
13 ³ Institute of Marine Sciences, National Research Council (ISMAR-CNR), Rome, Italy

14
15 ⁴ U. S. National Science Foundation National Center for Atmospheric Research (NSF NCAR), Boulder, CO, USA

16
17 ⁵ School of Earth and Environmental Sciences, Seoul National University, Seoul, South Korea

18
19 ⁶ NASA Goddard Institute for Space Studies (GISS), New York, New York, USA

20
21 ⁷ Canadian Centre for Climate Modelling and Analysis (CCCma), Victoria, British Columbia, Canada

22
23 ⁸ Met Office Hadley Centre, Exeter, United Kingdom

24
25 ⁹ Group of Meteorology, Universitat de Barcelona, Barcelona, Spain

26
27 ¹⁰ Barcelona Supercomputing Center (BSC), Barcelona, Spain

28
29 ¹¹ Faculty of Environmental Earth Science, Hokkaido University, Sapporo, Japan

30
31 ¹² Japan Agency for Marine-Earth Science and Technology, Yokohama, Japan

32
33 ¹³ Institute of Meteorology and Climate Research-Atmospheric Trace Gases and Remote Sensing (IMK-ASF) Karlsruhe
34 Institute of Technology (KIT), Karlsruhe, Germany

35
36 ¹⁴ Laboratoire de Météorologie Dynamique (LMD), Paris, France

37
38 ¹⁵ Meteorological Research Institute (MRI), Tsukuba, Japan

39
40 ¹⁶ National Centre for Atmospheric Science (NCAS), United Kingdom

41
42 ¹⁷ Department of Physics, University of Oxford, United Kingdom

43
44 ¹⁸ CMCC Foundation - Euro-Mediterranean Center on Climate Change, Italy

45
46 ¹⁹ Aichi University of Education, Kariya, Japan

47
48 ²⁰ Japan Agency for Marine-Earth Science and Technology (JAMSTEC), Yokohama, Japan

49
50
51 *Correspondence to:* Dillon Elsbury (delsbury@uci.edu)

52 **Abstract.** This study uses an ensemble of climate model experiments coordinated by the Quasi-Biennial Oscillation initiative
53 (QBOi) to analyze the Madden-Julian Oscillation (MJO) in the presence of either perpetual El Niño or La Niña sea surface
54 temperatures during boreal winter. In addition to the prescribed El Niño Southern Oscillation (ENSO) conditions, the nine
55 models internally generate QBOs, meaning each may influence the MJO. Objectives of our analyses are to assess the response
56 of the MJO to strong idealized ENSO forcing and look for evidence of a QBO influence on the MJO in a multi-model context.
57 The diagnostics used include wavenumber-frequency spectra of tropical convective and dynamical fields, measures of MJO
58 lifetime, an evaluation of MJO diversity and visualization of MJO vertical structure, as well as an assessment of QBO
59 morphology and the QBO’s impact on tropical convection. Kelvin wave spectral power increases in the El Niño simulations
60 whereas equatorial Rossby waves power is stronger in the La Niña simulations. All models simulate faster MJO propagation
61 under El Niño conditions. This change in speed is corroborated by the MJO diversity analysis, which reveals that models better
62 reproduce the observed “fast propagating” and “standing” MJO archetypes given perpetual El Niño and La Niña, respectively.
63 Regardless of ENSO, QBO descent into the lower stratosphere is underestimated and we detect little QBO influence on tropical
64 tropopause stability and MJO activity. With little influence from the QBO on the MJO activity in these runs, we can be
65 confident that the aforementioned changes in the MJO indeed arise from the different ENSO boundary conditions.

66 **1 Introduction**

67 The tropical circulation is influenced by various forms of internal variability, each operating at different timescales, yet still
68 influencing each other. The Madden-Julian Oscillation (MJO) is dominant at intraseasonal timescales (Madden and Julian
69 1994; Lin, 2022). It consists of large-scale eastward propagating fluctuations in tropical precipitation and circulation that
70 traverse the Indian Ocean and Maritime Continent through to the Pacific over roughly 30 to 60 days (Hendon and Salby 1994).
71 MJO variability fluctuates a lot year to year as does other variability in the climate system.

72
73 At interannual timescales, the El Niño Southern Oscillation (ENSO; Philander, 1990) is one of the most consequential sources
74 of tropical tropospheric variability. It is characterized by shifting patterns of sea surface temperatures (SSTs) and associated
75 changes in ocean and atmospheric circulations in the tropical Pacific. ENSO varies on timescales between two to seven years,
76 and consists of three phases, the warm El Niño, the cold La Niña and a “neutral” phase where neither polarity dominates. Also

77 operating at interannual timescales is the Quasi Biennial Oscillation (QBO), which is the dominant mode of variability in the
78 lower tropical stratosphere, defined by alternating easterly and westerly [zonal wind](#) shear zones descending from 5 to 100 hPa
79 with an average periodicity of 28 months (Baldwin et al. 2001).

80
81 The MJO, ENSO, and QBO are known to influence each other in various ways. ENSO's La Niña and El Niño phases are
82 associated with shifts of intraseasonal tropical atmospheric variability like the MJO towards the Indo-Pacific Warm Pool and
83 Date Line, respectively (Kessler 2001; Tam and Lau 2005). In addition, ENSO can influence the amount of time the MJO
84 spends in particular Wheeler and Hendon (2004) MJO phases and the duration of MJO events overall, which are shorter during
85 El Niño and longer during La Niña (Pohl and Matthews 2007; Pang et al. 2016; Wei and Ren 2019; Wang et al. 2019; Dasgupta
86 et al. 2021; Fernandes and Grimm 2023).

87
88 Nonetheless, not all research finds strong links between ENSO and seasonal-mean MJO activity. Slingo et al. (1999) found
89 that the observed intraseasonally filtered zonal mean 200 hPa zonal wind (their metric of "MJO activity") is weakly dependent
90 on ENSO phase. They affirmed this further by using an ensemble of AMIP simulations. Hendon et al. (1999) validated and
91 refined their definition of MJO activity, finding it to capture the salient features of the MJO and again that its variability is
92 mostly independent of ENSO. ~~With these results in mind, it is less clear how the MJO should respond to the ENSO conditions~~
93 prescribed in our simulations. In fact, a common idea amongst the studies just mentioned is that the MJO's interannual
94 variability originates predominantly from internal atmospheric processes other than those associated with ENSO.

95
96 It is increasingly recognized that the easterly and westerly phases of the QBO exert an influence on the MJO (Yoo and Son,
97 2016; Son et al. 2017; Sakaeda et al. 2020; Martin et al. 2021; Jin et al. 2023; Huang et al. 2023). The MJO's amplitude is
98 stronger during easterly QBO boreal winters compared to westerly QBO winters over the observed record since 1979 (Yoo
99 and Son 2016; Densmore et al. 2019). However, despite improvement in the representation of simulated QBOs (Richter et al.
100 2020) and MJOs (Ahn et al. 2020) across model generations, current free-running Earth system models generally do not
101 simulate the QBO-MJO relationship (Kim et al. 2020; Lim and Son 2020; Martin et al. 2023), nor do they simulate a
102 sufficiently strong tropical tropopause response to the QBO (Serva et al. 2022). Further complicating interpretation is a
103 tendency for easterly QBO boreal winters to co-occur with La Niña events, introducing ambiguity about the source of MJO
104 modulation (Randall et al. 2023).

105
106 In this study, we document the influence of ENSO on the MJO using a multi-model ensemble of idealized experiments with
107 perpetual El Niño and La Niña forcings. These simulations were coordinated by the Atmospheric Processes And their Role in
108 Climate (APARC, previously "SPARC") Quasi-Biennial Oscillation initiative (QBOi, Butchart et al. 2018). In addition to
109 prescribing ENSO, the models internally generate QBOs, meaning both types of interannual internal variability may modulate
110 the MJO in these experiments. Our aim is to assess the extent to which model behavior is consistent with previously reported

Deleted: These results also align with those of Newman et al. (2009) who showed that air-sea coupling has a small effect on intraseasonal atmospheric variability in empirical models that run with and without atmosphere-ocean interaction. ...

116 ENSO-MJO relationships, recognizing that past studies have found different ENSO-MJO links and that the simulated QBOs
117 may also project onto the MJOs. The coordinated QBOi protocol allows us to revisit these relationships in a controlled
118 framework that isolates atmospheric responses to fixed, high-amplitude ENSO SSTs across many models. These perpetual
119 ENSO conditions represent the strongest observed El Niños and La Niñas and offer an upper bound on ENSO’s effect on MJO
120 characteristics, providing a high signal-to-noise database for studying this connection. We also selectively incorporate Phase
121 1 QBOi experiments, performed as 1979-2009 Atmospheric Model Intercomparison Project experiments, and hence, more
122 representative of typical ENSO amplitudes (Butchart et al. 2018, Experiment 1). Unlike Coupled or Atmospheric Model
123 Intercomparison Project experiments, or historical reanalysis datasets, these simulations avoid complications associated with
124 time-evolving forcings, event-to-event ENSO variability, and background SST biases. On the other hand, while perpetual
125 ENSO conditions help isolate atmospheric responses, they also preclude direct comparison with observation-based datasets,
126 which include event-to-event variability, for example. The perpetual-ENSO experiments used here are a continuation of the
127 QBOi Phase 1 experiments and have companion studies that examine ENSO’s effect on the QBO (Kawatani et al., 2025) and
128 the combined influence of ENSO and the QBO on global teleconnections (Naoe et al., 2025).

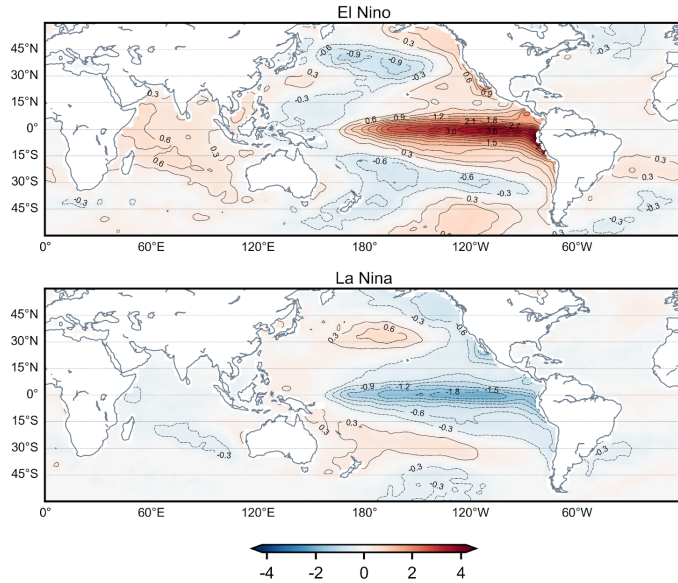
129 **2 Methods**

130 **2.1 Experimental setup**

131 Butchart et al. (2018) established a set of simplified modeling experiments for Phase 1 of the QBOi. Their Experiment 2, the
132 “present-day time slice” simulation, forms the basis for these perpetual ENSO simulations. It was designed to allow for an
133 evaluation of the accuracy of modeled QBOs under present-day conditions, that is, how the model QBOs operate in a climate
134 forced with fixed repeating annual cycles of global sea surface temperature (SSTs), sea ice concentration (SIC), and external
135 forcings representative of the time averaged 1988-2007 state.

136
137 The perpetual ENSO runs analyzed here are equivalent to Experiment 2, but with global El Niño or La Niña SST anomalies
138 superimposed on top of the climatological SST forcing. An assessment of the MJO is not conducted for Experiment 2 because
139 essential variables such as daily horizontal winds, outgoing longwave radiation (OLR), and precipitation, were not archived.
140 In creating the composite El Niño or La Niña forcings, the characterization of ENSO follows the Japan Meteorological Agency
141 (JMA) convention, where ENSO is defined by the spatially averaged NINO.3 (5°S-5°N, 150°W-90°W) monthly SST anomalies
142 from 1950-2016. Anomalies are defined as deviations from the climatological seasonal cycle and computed relative to the
143 most recent sliding 30-year period of JMA COBE-SST version 1 data (JMA, 2006). The anomalies are smoothed using a five-
144 month running mean and the periods during which the anomalies exceed 0.5°C (-0.5°C) for at least six consecutive months
145 are labeled as El Niño (La Niña) periods. However, after averaging the SST anomalies for all El Niño Januarys, Februarys,
146 etc., and doing the same for La Niña, the composite average annual cycles of El Niño and La Niña SSTs show only modest
147 amplitudes (e.g., 1.92 °C for El Niño Januarys). To amplify the atmospheric response to ENSO in the simulations and increase

148 the signal-to-noise ratio, the annual cycles are multiplied by 1.8 and 1.4, respectively, making their amplitudes comparable to
149 the strongest observed ENSO events. A similar scaling is applied to the corresponding global signatures in NINO.3 SST
150 anomalies (Fig. 1), which are superimposed on 1988–2007 climatological SSTs and prescribed in the models. Note that this
151 procedure does not completely capture the development, mature phase, and decay of all observed El Niño events, due to
152 diversity in the evolutions of events. We refer the reader to Kawatani et al. (2025) for more details on the experimental design
153 and sensitivity of the model QBOs.



154
155 **Figure 1: November-April composites of the El Niño (top) and La Niña (bottom) JMA COBE SST anomalies (units K) that are**
156 **prescribed in the perpetual ENSO simulations.**

157 In addition to the prominent El Niño and La Niña signals, the November-April (NDJFMA) SSTs shown in Figure 1 include
158 the signatures of the basin-scale Interdecadal Pacific Oscillation (IPO) (Henley et al. 2015) and Indian Ocean SSTs that are in
159 phase with ENSO. In some regions like the tropical Pacific and Indian Oceans, the amplitude of the global SSTs associated
160 with the El Niño are roughly double that of La Niña (Fig. 1).

161
162 **2.2 Models**

163

164 *Table 1*: The models used in this study, the horizontal (given as spectral triangular truncation, T , or longitude-latitude increments) and
 165 vertical configuration (number of levels and model top, in hPa), the number of years per simulation, and relevant literature for the convective
 166 schemes. Only one realization is used from each model.

Model	Horizontal resolution	Vertical levels (top, hPa)	Number of years	Convective parameterizations
EC-EARTH3.3	T255	91 (0.01)	101	Bechtold (2014)
ECHAM5sh	T63	95 (0.01)	40	Tiedtke (1989), Nordeng (1994)
EMAC	T42	90(0.01)	106	Tiedtke (1989)
LMDz6	2°-1.25°	79 (0.015)	80	Emanuel (1991), Hourdin et al. (2013)
GISS-E2-2-G	2°-2.5°	102 (0.002)	30	Rind et al. (2020); Kelley et al. (2020)
MIROC-AGCM-LL	T106	72 (1.2)	100	Pan and Randall (1998); Emori et al. (2001)
MIROC-ESM	T42	80 (0.0036)	100	Pan and Randall (1998); Emori et al. (2001)
MRI-ESM2.0	T159	80 (0.01)	50	Yukimoto et al. (2019)
CESM1(WACCM5-110L)	1.25°-0.94°	110 (6.1E-6)	101	Zhang and McFarlane (1995)

Commented [FS1]: I've changed the vertical column a bit to avoid repetition

167
 168 The models considered are listed in Table 1 along with the number of years analyzed for each model and references on each
 169 model's convective parameterization. These parameterizations impact the representation of tropical phenomena (Holt et al.
 170 2020; Kawatani et al., 2025), including the simulation of intraseasonal oscillations (Ham and Hong, 2013). For example, past
 171 sensitivity tests with the version of MIROC-ESM that we use here have shown that its cumulus parameterization struggles to
 172 simulate an MJO of realistic amplitude with capability to propagate over the Maritime Continent (Miura et al. 2012). The
 173 updated scheme (Chikira and Sugiyama 2010) in use in newer versions of the model, MIROC6, has helped ameliorate these
 174 issues (Ahn et al. 2017; 2020). The importance of simulated convection-circulation coupling has been identified for other
 175 models (Kim et al. 2014; Zhu et al. 2020; Wang et al. 2022).

176 **2.3 Observation-based reference data**

177 To be consistent with previous studies (e.g., Wei and Ren 2019), the ENSO-MJO relationship is considered during
178 November-April. The six historical La Niña years, where the year is associated with November, are 1970, 1984, 1988, 2017,
179 2020, and 2021 and the eight El Niño years are 1968, 1982, 1986, 1991, 1997, 2009, 2015, 2018. Each corresponds to an
180 instance when the smoothed Niño3 anomalies exceed $\pm 0.5^\circ\text{C}$ for at least six consecutive months. For comparison with the
181 models, the subsequent analyses include “observed” El Niño and La Niña composites, formed by averaged deseasonalized
182 1959-2022 ERA5 reanalysis (Hersbach et al. 2020) over the years. Unlike the model simulations, which prescribe ENSO
183 SST anomalies scaled by factors of 1.8 (El Niño) and 1.4 (La Niña), the ERA5 composites reflect unscaled, event-based
184 variability. While this distinction makes direct comparison between models and reanalysis imperfect, ERA5 nonetheless
185 provides a useful benchmark for expected atmospheric responses. The ERA5 El Niño and La Niña composites are best
186 interpreted in relation to each other, rather than as strict analogs to the simulations.

187 Satellite-based daily precipitation estimates from a 1996-2023 Global Precipitation Climatology Project (GPCP, v1.3) record
188 (Huffman et al. 2001; Adler et al. 2017) are used to assess ENSO-related precipitation anomalies, as is NOAA Interpolated
189 Outgoing Longwave Radiation (Liebmann and Smith 1996). For these analyses, El Niño and La Niña years are defined as
190 ± 1 variations in standardized November-April Niño3 anomalies, yielding 1997, 2009, and 2015, and La Niña years as
191 1999, 2007, and 2010. Unlike ERA5, where cloud fields and precipitation are parameterized without direct assimilation,
192 satellite-based datasets provide a more direct observational reference, particularly valuable in the tropics where reanalysis
193 precipitation is known to be less reliable (Gehne et al. 2016).

194 **2.4 MJO analyses**

195 We implement a number of widely-used methods to evaluate the MJO in the perpetual ENSO simulations. In the interest of
196 exploring changes to MJO lifetime by ENSO phase as well as visualizing the MJO’s vertical structure, we compute Real-time
197 Multivariate MJO indices (RMMs) for each perpetual ENSO simulation using a similar methodology to Wheeler and Hendon
198 (2004, WH04). The RMMs are derived from a combined empirical orthogonal function (EOF) analysis of tropically averaged
199 (15°S - 15°N) anomalous daily outgoing longwave radiation (OLR), 200-hPa zonal wind (U200), and 850-hPa zonal wind
200 (U850). As in WH04, we deseasonalize, remove interannual variability, and normalize the anomalies by their global variance.
201 To enable a fairer comparison between the models and reanalysis, we project the anomalous model fields onto 1959-2022
202 ERA5 WH04 EOFs, which are computed by using ERA5 winds and ERA5 OLR; projecting onto each model’s respective
203 ENSO simulation instead does not change the conclusions and using NOAA OLR in the EOFs has minimal impact on model
204 the RMMs (not shown). Daily OLR and U200 were not available for two models (GISS-E2-2-G and LMDz6) so their RMMs
205 are computed using U250 and U850.

Deleted: the same

Deleted: as

Deleted: the

Deleted: As observation-based reference, the RMMs are computed by using the ERA5 wind and the

Deleted: OLR fields.

213 The number of MJO events within a given data set is tallied like in Pohl and Matthews (2007) by counting the number of times
214 the MJO makes a complete rotation through its RMM1 and RMM2 phase space. Average lifetime and MJO amplitudes
215 ($\sqrt{(RMM1^2) + (RMM2^2)}$) are computed across events. To visualize the MJO's vertical structure, latitudinally averaged
216 10°S-10°N longitude-pressure cross-section of zonal wind and temperature are projected onto the RMMs using the same steps
217 as Hendon and Abhik (2018), but applied across ENSO years in the present study rather than QBO years.

219 The MJO is visualized using two related wavenumber–frequency approaches. Both Fourier ~~transform~~ deseasonalized and
220 detrended, highpass filtered, tapered time-longitude data, reorder coefficients into eastward/westward components, and
221 compute power spectra to isolate intraseasonal variability. The CLIVAR/MJO metric (Waliser et al. 2009) applies this to
222 centered November-April segments of tropical U850, yielding single variable power for eastward and westward disturbances
223 (Figure 3). The Wheeler and Kiladis (1999) style analysis is similar, but designed to diagnose the broader family of
224 convectively coupled equatorial waves alongside the MJO: we linearly detrend multiyear daily fields, highpass filter at 96 days,
225 use overlapping 96-day segments (65-day overlap), perform successive longitude–time transforms, recover symmetric and
226 antisymmetric spectra about the equator, and normalize by a smoothed background; results are presented as the ratio of raw
227 symmetric daily mean precipitation power to background (Figure 2). Our Wheeler-Kiladis implementation also subsets data
228 to November-April. For model evaluation, spectra are divided by each model's perpetual ENSO background, whereas GPCP
229 (ERA5) El Niño and La Niña spectra are compared to a common 1996-2022 (1959–2022) background.

231 We also implement an MJO diversity analysis in which MJO events are classified into distinct types based on their propagation
232 characteristics using k-means clustering (Wang et al. 2019). Each MJO event is binned as one of four archetypes, “standing”
233 or “jumping” MJOs, which propagate across the Indian Ocean, but are distinguished by reemergence of the MJO over the
234 western Pacific during jumping events, and “slow” or “fast” MJOs, which both continuously propagate across the Maritime
235 Continent, but at different speeds. An MJO event occurs when the 20-70 day bandpass-filtered OLR anomalies (from seasonal
236 cycle) averaged over the equatorial Indian Ocean (10°S-10°N, 75°E-95°E) are smaller than negative one standard deviation
237 for five successive days; the reference day (day 0) is the day of minimum OLR. The MJO events are categorized by a k-means
238 clustering of the enhanced convective signal (OLR anomalies under -5 Wm^{-2}) of the latitudinally averaged 10°S to 10°N time-
239 longitude OLR anomalies taken over 60°E to 180°E and over a 31-day period from day -10 to day 20. For brevity, we omit
240 further diversity analysis methodological details, for which we refer the reader to Back et al. (2024) for all steps. Unlike Wang
241 et al. (2019), in which initial centroids for clustering are randomly chosen, initial centroids for model MJO events are set to
242 those of the four observation-based clusters, allowing the present study to evaluate how well climate models reproduce
243 observed MJO diversity with minimal subjectivity.

Commented [FS2]: something's wrong with this formula. I suggest using something like "summed in quadrature" or similar

Commented [FS3R2]: mm, the change in formula can't be tracked

Deleted: transform

Commented [FS4]: We might mention that this choice may artificially introduce power around 180 days

Commented [de5R4]: True. I added this, but put it in the caption beneath Figure 3

Deleted: To sharpen the MJO and facilitate comparison with the CLIVAR metric, o

Deleted: GCPP

Deleted: ; GPCP and ERA5 conclusions are insensitive to using regime specific backgrounds.

250 **2.5 QBO and analyses**

251 The space-time form of the QBOs varies from model to model as each is generated with different amounts of forcing from
252 resolved waves and parameterized non-orographic gravity wave drag. Properties of these models that are particularly relevant
253 for simulating the QBOs are listed in Butchart et al. (2018), details on QBO morphology (e.g., its amplitude, latitudinal width)
254 given the observed SST record are presented in Bushell et al. (2022), and the relative contribution of resolved and
255 parameterized tropical waves to forcing the QBO is analyzed in detail in Holt et al. (2020). Of note, MIROC-AGCM-LL's
256 QBO is forced solely by resolved waves. As EC-EARTH and GISS-E2-2-G did not contribute to some of the earliest QBO
257 analyses, relevant details on their internal QBOs can be found in Serva et al. (2024) and Rind et al. (2014, 2020), respectively.
258 For a thorough analysis of how the QBO responds to the perpetual ENSO simulations, we refer the reader to Kawatani et al.
259 (2025).

260
261 To help clarify the ability of the QBOs to interact with the MJOs, we use established metrics to characterize the morphology
262 of the ERA5 and model QBOs. The main field used to document QBO morphology is the monthly zonal-mean zonal wind.
263 "QBO cycles" (consecutive easterly/westerly phases) are identified by marking the first month when the deseasonalized and
264 smoothed (5-month running mean) 20 hPa 5°S-5°N wind changes from westerly to easterly, ending one month before the next
265 transition at 20 hPa (Kawatani et al. 2019). From these cycles, we calculate average QBO easterly, westerly, and total
266 amplitudes using the QBO "transition time" methodology of Richter et al. (2020). The easterly (westerly) amplitude is equal
267 to the average of the minimum (maximum) monthly QBO winds from each QBO cycle. The QBO cycles are used further to
268 calculate minimum, mean, and maximum QBO periodicity statistics. These statistics are a key result of Kawatani et al. (2025)
269 and are discussed thoroughly there. In short, the periodicity of the QBO decreases in all El Niño simulations and increases in
270 all La Niña simulations, which is attributed to ENSO modulating convection and the low-frequency circulation, thereby
271 influencing generation of tropical waves and their filtering by the large-scale circulation and the QBO. For the purposes of the
272 present study, the minimum and maximum periodicities are required to evaluate the QBO's spatial structure, defined as the
273 latitude-pressure cross sections of each data set's QBO Fourier amplitude. These are made by applying a discrete Fourier
274 transform in time to the multi-year monthly zonal-mean zonal wind at each pressure-latitude grid point and dividing the sum
275 of squares of the amplitudes of the harmonics corresponding to periods between the minimum and maximum QBO periods by
276 the sum of squares of the amplitudes of all harmonics. This ratio is subsequently multiplied by the standard deviation of the
277 zonal-mean zonal wind (Pascoe et al. 2005). Using this QBO Fourier amplitude, the lowest altitude the QBO reaches, its
278 vertical extent (i.e., how tall it is), and its latitudinal extent are defined as in Schenzinger et al. (2017), except that here the
279 QBO's maximum amplitude is assumed to be at 20 hPa for all models and ERA5.

280
281 QBO impact on the MJO is assessed using the techniques of Klotzbach et al. (2019) and Kim et al. (2020). Following the prior,
282 we make scatterplots of December-February warm-pool (10°S-10°N, 45°E-180°E) averaged tropopause stability (100 hPa

283 minus 200 hPa temperature) versus December-February MJO amplitude as a function of QBO phase (sign of DJF averaged
284 5°S-5°N 50 hPa zonal mean zonal-wind) for each of the simulations. MJO amplitude is expected to increase as tropopause
285 stability decreases, which happens during the easterly QBO phase. As in Kim et al. (2020), MJO activity is also computed as
286 a function of QBO phase. Specifically, MJO-filtered OLR is calculated following Wheeler and Kiladis (1999) with one
287 exception, the full time series is detrended rather than using 96-day overlapping segments. To minimize spectral leakage, 5%
288 of the data are tapered to zero at the ends of the timeseries. After tapering, a complex Fourier Transform is performed, and the
289 spectral wavenumber-frequency data are filtered to retain only the eastward propagating coefficients for 20-100 day periods
290 and wavenumbers 1-5. MJO activity is then defined as the standard deviation of the MJO-filtered OLR across all December-
291 February days that fall into a particular category, for instance all years, easterly QBO years or westerly QBO years. For this
292 analysis, easterly and westerly QBO years are defined as those which exceed +/- 0.5 standard deviation of the 50 hPa monthly
293 zonal wind anomalies, seasonally smoothed and averaged over 10°S to 10°N. We allow the QBO to be defined differently
294 between the Klotzbach and Kim et al. analyses; here we prioritize using the aforementioned metrics in their original form
295 rather than using customizing them.

Deleted: A

296 3 Results

297 3.1 Impact of perpetual ENSO conditions on the MJO,

Deleted: ENSO

298 3.1.1 Role of convectively coupled waves

Deleted: -MJO interaction

Formatted: Normal

299 Before examining the influence of ENSO on MJO, we evaluate some of the other large-scale tropical phenomena that the
300 models simulate. Convectively coupled waves are relevant because they comprise the space-time structure of the MJO and can
301 influence its propagation by modulating the tropical circulation and the distribution of moisture that the MJO encounters
302 (Kiladis et al. 2009; Wang et al. 2019; Wei and Ren 2019; Berrington et al. 2022; Wang and Li 2022). Aspects of the waves,
303 such as their phase speed and what longitudinal domain they propagate in, vary depending on the seasonal-mean circulation
304 and convective activity (Roundy 2012; Yang et al. 2023). Hence, the amplification of the Walker Circulation by La Niña and
305 the weakening of it by El Niño (Fig. S1) provide a pathway for the perpetual ENSO forcings to modulate the waves and perhaps
306 the MJO. Applying similar methods to Wheeler and Kiladis (1999), we visualize the waves by computing the spectral power
307 of GPCP, ERA5, and model daily-averaged precipitation as a function of wavenumber and frequency. Figure 2 shows the
308 precipitation spectra for phenomena symmetric about the equator, taken over November-April and 15°S-15°N. Three
309 dispersion curves, as in Matsuno (1966), corresponding to equivalent depths of 10, 25, and 50 meters are also superimposed;
310 these curves are derived using the dispersion relations for equatorially trapped waves and they are co-located with modes of
311 organized convection, with larger equivalent depths corresponding to faster phase speeds.

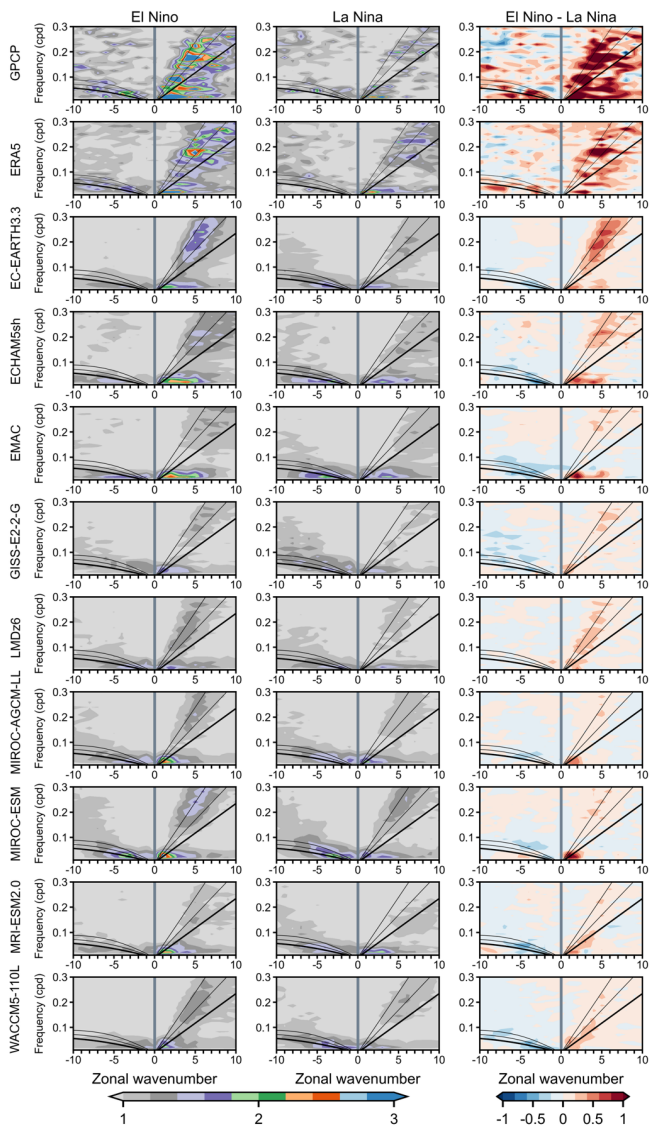
Deleted: low frequency

312
313 The GPCP panels in row one draw on only three La Niña and three El Niño years, while the ERA5 panels in row two use just
314 six La Niña and eight El Niño years, resulting in signals that are noisier than the models' multi-decade averages. Power is

319 typically the highest amplitude in GPCP, then ERA5, and weakest in the models. Spectral signals associated with the eastward
320 propagating Kelvin wave move up and to the right on each panel, spanning sub-planetary low frequency ($\sim k = 3, 25$ days)
321 scales to synoptic ($k = 4+$) sub-weekly scales. Relative to GPCP and ERA5, the models underestimate the strength of the
322 Kelvin wave, irrespective of the type of ENSO forcing, but have worse difficulties in the El Niño simulation. Power associated
323 with the westward propagating equatorial Rossby wave is evident on the left side of each panel between wavenumbers 1-10
324 and timescales of 10 days to five weeks. Overall, the models do a reasonable job of simulating the spectral amplitude of
325 equatorial Rossby waves, although it is too strong for some models (EMAC, MIROC-ESM), especially in their La Niña
326 simulations.

327

Deleted: -



330 **Figure 2:** Wavenumber-frequency spectrum of the symmetric component of 15°S–15°N November–April precipitation plotted as the
331 ratio between raw symmetric precipitation and a smoothed red noise background spectrum. The eastward (right) side of the
332 spectrum includes three Kelvin wave dispersion curves in black, of which the thickest curve corresponds to the equivalent depth of
333 12 meters, and the others to 25 and 50 meters, respectively. Similar dispersion curve plotting conventions are used on the westward
334 (left) side of the spectrum where the curves overlay the equatorial Rossby wave power. Column one corresponds to El Niño, column
335 two to La Niña, and column three to their difference, which is computed as (El Niño symmetric/El Niño background) minus (La
336 Niña symmetric/La Niña background). Computing the third column as (El Niño symmetric) minus (La Niña symmetric) yields
337 similar conclusions (not shown).
338

339 3.1.2 ENSO effects on convectively coupled waves,

340 The effect of ENSO phase on each wave is revealed by the rightmost column of Figure 2, which shows El Niño (column one)
341 minus La Niña (column two) differences, where red means stronger power during El Niño and blue means larger power during
342 La Niña. All models simulate stronger Kelvin waves in their El Niño simulation, particularly along the deeper equivalent depth
343 ($n = 25, 50$ meters) dispersion curves. This implies faster Kelvin wave phase speeds during El Niño. Examining the El Niño
344 column, the alignment of the Kelvin wave power along these particular curves is demonstrated by EC-EARTH3.3, GISS-E2-
345 2-G, LMDz6, MIROC-AGCM-LL, MIROC-ESM, MRI-ESM2.0 and (CESM1) WACCM5-110L, hereafter just “WACCM5-
346 110L.” The remaining models, ECHAM5sh and EMAC (both ECHAM-based models), differ in that their El Niño Kelvin wave
347 power is weighted towards higher zonal wavenumbers for frequencies below 0.2 cpd. GPCP and ERA5 shows large sporadic
348 increases in Kelvin wave power along deeper equivalent depth dispersion curves during El Niño compared to La Niña. It is
349 suggested that the Kelvin wave intensifies during observed El Niños because SST-driven increases in equatorial convection,
350 combined with a weakened upper-tropospheric westerly duct over the eastern Pacific, enhance the convective and dynamical
351 coupling that supports Kelvin wave growth. La Niña produces the reverse effect (Yang and Hoskins 2013; Yang et al. 2023).

352
353 In contrast, for the westward propagating equatorial Rossby wave, GPCP and ERA5 indicate stronger power during El Niño,
354 whereas all models simulate stronger Rossby wave power during La Niña. This discontinuity arises with models having weaker
355 El Niño Rossby wave spectral power than the GPCP and ERA5 composites (not shown), but stronger power given the La Niña
356 forcing. It should be noted that equatorial Rossby waves exhibit strong regional variations in observations, varying with the
357 strength and position of seasonal-mean tropical westerlies and in response to extratropical Rossby waves entering low latitudes
358 (Yang and Hoskins 2016) factors we do not examine here. Such regional impacts may help explain why the GPCP and ERA5
359 composites differ from the model-simulated ENSO responses. Our observed composites show some consistency with Yang et
360 al. (2023) who found stronger equatorial Rossby waves during El Niño when the satellite-based OLR spectra were restricted
361 to the western hemisphere (their Fig. 13).

362
363 The ENSO-related differences in convectively coupled waves highlighted above motivate investigation into whether the MJO,
364 as represented in the models, also varies systematically by ENSO phase. Observational and modeling studies report that ENSO
365 modulates MJO propagation, amplitude, and regional impact, with notable differences in MJO structure between El Niño and

Commented [FS6]: there is something strange with Figure 2...are there two images overlapped?

Commented [FS7R6]: the one in background seems to have lower resolution

Commented [de8R6]: Yes, the old Figure was in the background - i deleted it

Deleted:

Deleted: minus

Deleted: minus

Formatted: Font: Bold

Deleted: Similar to the models,

Commented [FS9]: add <https://journals.ametsoc.org/view/journals/atsc/70/11/jas-d-13-081.1.xml>

Deleted:

Deleted: from

Deleted: underestimating

Deleted: average equatorial

Deleted: t

Deleted: or

Deleted: during El Niño

Deleted: while overestimating

Deleted: power

Deleted: during

Deleted: relative to GPCP and ERA5 (not shown).

Deleted: also

Deleted: the response of

Deleted: -gravity

Deleted: has

Deleted: larger

Deleted: , at least

Deleted: investigate this circumstance in this work. Indeed,

Commented [de11R10]: Thanks for this addition. I am going to move this to discussion/conclusion as its impact is stronger there.

Deleted: ¶

Deleted: ¶

Deleted: Yang

Deleted: et al. (2023) also highlighted the role of ENSO-mediated changes in the zonal flow, which was found (... [1])

403 [La Niña \(Wei and Ren 2019; Fernandes and Grimm 2023\)](#). This raises the question of whether the model MJOs analyzed here
404 [capture these ENSO-dependent features, a topic addressed in the next section.](#)

406 **3.1.3 MJO representation and ENSO dependence**

407 Having found changes in the convectively coupled waves due to ENSO, perhaps the model MJOs also behave differently given
408 ENSO state. Broadly speaking, Figure 2 shows that the models include MJOs as indicated by the maxima in spectral power at
409 intraseasonal timescales ($\ll 0.1$ cpd) between eastward propagating wavenumbers 1-5. Holt et al. (2020) also found MJOs to
410 be simulated by these models in historical AMIP simulations (QBOi Exp 1). The highest MJO power in GPCP is concentrated
411 between wavenumbers 1 and 3 [irrespective of ENSO phase](#) and exceeds that of ERA5 and the models. [The ENSO simulations](#)
412 [for EC-EARTH3.3, MIROC-AGCM-LL, MIROC-ESM, MRI-ESM2.0](#) correctly position MJO power between wavenumbers
413 1-3 whereas ECHAM5sh, EMAC (sharing convective parameterizations) and [LMDz6](#) exhibit spectral power that is incorrectly
414 shifted towards higher wavenumbers. The amplitude of the MJO is comparatively small in GISS-E2-2-G, LMDz6, and
415 WACCM5-110L, which may adversely affect their stratospheric waves, since these three models adopted interactive GW
416 sources. The El Niño minus La Niña differences in the rightmost column of Figure 2 show that MJO spectral power is stronger
417 in the presence of the El Niño basic state. Differing from the other models, EC-EARTH3.3, ECHAM5sh, and EMAC have
418 fairly large El Niño minus La Niña MJO power differences at wavenumber 4 and 5.

419
420 Irrespective of ENSO phase, the amplitude of the model MJOs as shown in Fig. 2 is systematically weaker than in GPCP or
421 ERA5. This may have something to do with dividing each simulation's symmetric power by its respective background power,
422 the latter of which is contaminated, in a sense, by the perpetual ENSO conditions. Note that recomputing the third column of
423 Fig. 2 without dividing each El Niño and La Niña composite by their respective background does not change our conclusions
424 (not shown). To get around this potential issue with the background power and further inspect the model MJOs as opposed to
425 the convectively coupled waves, in Figures 3 we consider the westward and eastward wavenumber-frequency spectra of U850
426 taken over the intraseasonal timescale and over MJO-like zonal wavenumber scales. These analyses yield more holistic views
427 of the MJO than in Fig. 2 because they incorporate the MJO's signals in these fields that are both symmetric and antisymmetric
428 about the equator.

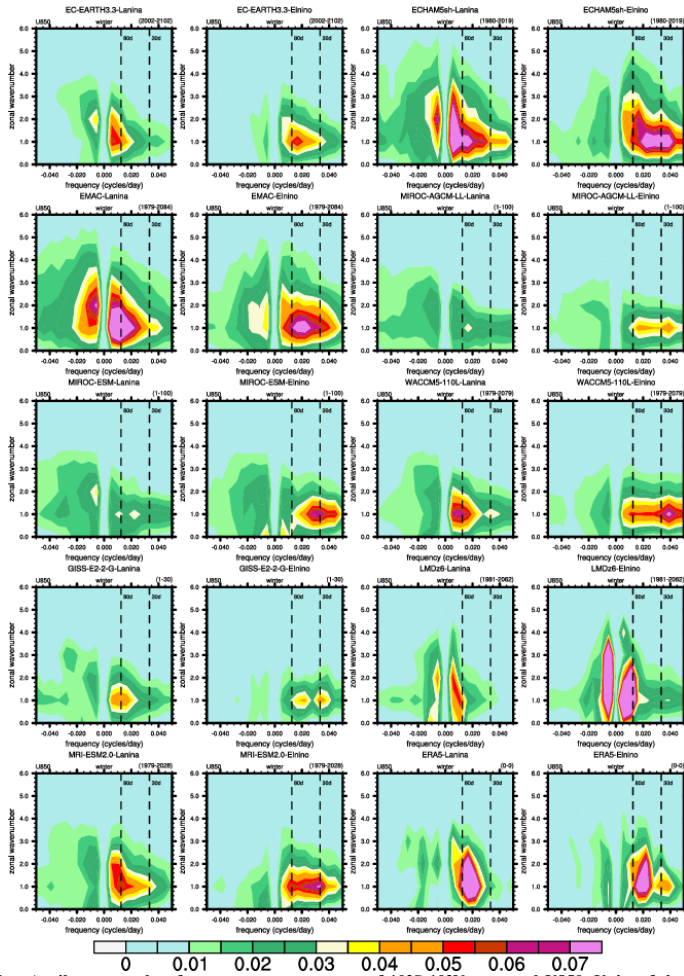
Deleted: ¶

Formatted: Font: Bold

Commented [FS12]: to check: may cite this one DOI
10.1007/s00382-012-1343-y for LMDz poor MJO

Commented [FS13R12]: maybe not to cite, but I found a
few MJO works where LMDz is
nudged...<https://agupubs.onlinelibrary.wiley.com/doi/full/10.1002/2015JD023461> we could mention MJO/QBO nudging
in Discussion section?

Commented [de14R12]: Omitting this for brevity



431
 432 **Figure 3:** November-April wavenumber-frequency power spectra of 10°S-10°N averaged U850. Units of the U850 spectrum are
 433 m²/s² per frequency interval per wavenumber interval. We interpret the power at ~ 180-day frequencies as a by-product of using
 434 centered November-April segments.
 435

436 As shown by ERA5, the MJO timescale variance of dynamical fields such as U850 are known to have a narrow spectral peak
 437 around zonal wavenumber-1 (Hendon and Salby 1994). The models are fairly good at reproducing this (Fig. 3), despite large

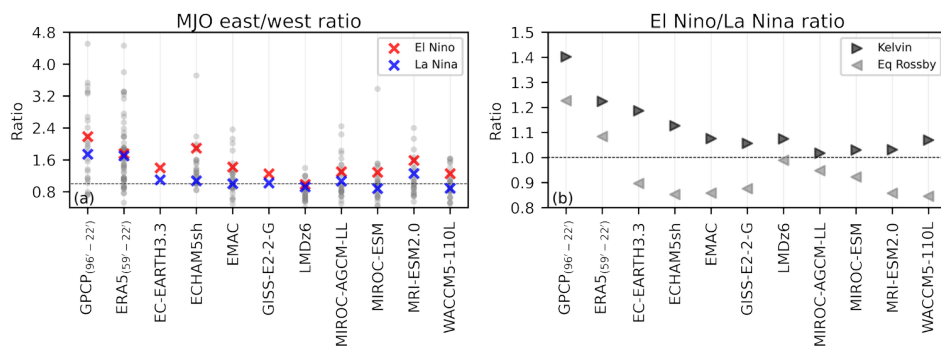
438 inter-model differences in terms of peak amplitudes. Independent of the ENSO phase, ERA5's wavenumber-frequency shows
 439 the highest power between frequencies of 30-80 days (vertical dashes), a so-called "MJO band" (Ahn et al. 2017). Considering
 440 only the ERA5 MJO band, the MJO is stronger given lower zonal wavenumbers and longer periodicities during La Niña
 441 compared to El Niño. Similarly, the model spectra broadly indicate that the periodicity of the MJO decreases during El Niño
 442 and increases during La Niña. However, as was the case for the symmetric precipitation spectra (Fig. 2), there are notable
 443 differences in the amplitude of the spectral power between models and reanalysis. Of the models, MJO band amplitude in
 444 ECHAM5sh and EMAC is most like ERA5, whereas other models, particularly MIROC-AGCM-LL, MIROC-ESM, and
 445 GISS-E2-2-G significantly underestimate the strength of the MJO in this metric. Another issue is that models exhibit too large
 446 of an MJO signal for zonal wavenumbers three and up, which is unrealistic and common amongst GCMs (Ahn et al. 2017),
 447 with exaggerated high-wavenumber amplitudes in ECHAM5sh, EMAC, and LMDz6, as previously noted for precipitation.
 448 The clustering of models related to each other, such as MIROC and ECHAM-based models, affirm that the tropospheric wind
 449 response to imposed ENSO anomalies is strongly influenced by model configuration and convective schemes.

Deleted: s

Deleted: particularly

Deleted: indicate

Deleted: also



452 **Figure 4:** (a) Ratio of eastward to westward MJO precipitation spectral power (from Figure 2) filtered for wavenumbers +/- 1 to 3
 453 and 30 to 96 day frequencies. Red and blue X's denote El Niño and La Niña, respectively, using the same notation for both the GPCP
 454 and ERA5 composite averages and the climatological values from the perpetual El Niño and La Niña simulations. Gray dots indicate
 455 interannual east/west ratios from GPCP, ERA5, and the QBOi Experiment 1 simulations (1979-2009 AMIP) by these same models;
 456 EC-EARTH3.3 and GISS-E2-2-G did not run Experiment 1. (b) Ratio of Kelvin wave and equatorial Rossby wave power in El Niño
 457 to that in La Niña. Each wave is filtered using equivalent depths of 8 to 90 meters, with wavenumbers of 1 to 14 for the Kelvin wave
 458 and -1 to -10 for the equatorial Rossby wave.
 459

460
 461 To further explore the MJO timescale changes suggested by Figure 3, Figure 4a shows the ratio of eastward to westward MJO
 462 spectral power in symmetric precipitation from GPCP, ERA5, and the models. The E/W ratio measures how robust MJO
 463 eastward propagation is (Jiang et al. 2015; Ahn et al. 2017). El Niño and La Niña responses in GPCP and ERA5 (red and blue
 464 X's) are derived from composites of previously defined strong ENSO seasons, while gray dots represent interannual E/W

Commented [FS15]: @Dillon please revise this caption!

Commented [FS16R15]: I guess we could say that tropical waves sensitivity is better reproduced than MJO by comparing these plots, right?

Commented [de17R15]: We could say that, but it's more true for some models (GISS, LMDz6), no? For ECHAM5sh (assuming its mean E/W ratio is ~ 1.5), the ENSO forcings drive a ~30% shift in ratio, whereas ECHAM5sh's Kelvin/ER changes are maybe ~ 15%. What do you think? I do want to write something along these lines, comparing panel (a) vs. (b)

Commented [FS18R15]: Yes, that's a good idea. I cited Laura's paper as RG waves are less well simulated than K waves.

Commented [FS19]: how come this paragraph is not track changed?

Commented [de20R19]: It was pasted in using editing mode, not reviewing mode

Formatted: Line spacing: 1.5 lines

469 ratios across all years (GPCP: 1996–2022; ERA5: 1959–2022), providing a baseline of internal variability. Both data sets show
 470 modestly higher E/W ratios during El Niño than La Niña.

471 It is worth iterating that the models' ratios are derived from the climatological means of the perpetual ENSO simulations, in
 472 contrast with the event-based composites of GPCP and ERA5. Model gray dots are interannual ratios from QBOi Experiment
 473 1 AMIP 1979-2009 simulations, which contextualizes internal variability. E/W ratios are higher in El Niño simulations,
 474 shifting towards the upper tail of the AMIP-based sampling variability. Conversely, many of La Niña E/W ratios are around
 475 one (dashed line), indicating subdued MJO propagation. The response to ENSO is relatively small in models with a weak
 476 MJO, such as GISS, LMDz6 and MIROC-AGCM-LL.
 477

478
 479 Building on the observed ENSO-related changes in MJO propagation, Figure 4b further quantifies how convectively coupled
 480 equatorial waves, Kelvin and equatorial Rossby, respond to ENSO forcing, given their known links to MJO variability. Figure
 481 4b shows the ratio of El Niño to La Niña precipitation-based spectral power, filtered from Figure 2 for each wave type. GPCP
 482 and ERA5 composites indicate that both waves are stronger during El Niño than La Niña. Models generally reproduce stronger
 483 Kelvin waves in their El Niño simulations. However, equatorial Rossby waves are consistently stronger in La Niña simulations,
 484 in contrast to GPCP and ERA5. This disagreement between observational products and models is difficult to attribute given
 485 the differences in how spectra for each are computed and known biases in modeled precipitation spectra (Holt et al. 2020,
 486 Experiment 1). This discrepancy arises with model equatorial Rossby waves being weaker in the El Niño simulation than in
 487 GPCP and ERA5, but stronger than the observational benchmarks in the La Niña simulation (not shown).
 488

489 The modulation of Kelvin and equatorial Rossby wave activity by ENSO, as evidenced in the historical records and models,
 490 is expected to impact the MJO's propagation speed and spatial structure (Wang et al. 2019). Since the balance between these
 491 waves impacts the MJO's eastward progression, it is helpful to assess how such dynamical changes are reflected in the
 492 statistical properties of MJO events, specifically their lifetime and diversity, across different ENSO backgrounds.

493
 494 *Table 2: The number of MJO events, their mean lifetimes and standard errors (reported in parentheses), and their mean amplitudes given*
 495 *either perpetual El Niño or La Niña conditions in a model. An asterisk (*) next to a model name indicates that the RMMs were retrieved*
 496 *using only 250 and 850 hPa zonal wind. Different from the models, for ERA5, MJO event statistics are calculated using 8 El Niño and 6 La*
 497 *Niña winters subsampled from the entire 1959-2022 RMM record.*
 498

	EN events (#/dec)	LN events (#/dec)	EN lifetime (days)	LN lifetime (days)	EN amplitude	LN amplitude
ERA5	25	22	38.25 (2.27)	47.07 (3.97)	1.36	1.41

Deleted: T

Commented [de22R21]: Yes, all new

Commented [FS23]: or inter-annual?

Commented [de24R23]: yeah I think inter-annual makes more sense

Deleted: While

Deleted: the model ENSO responses in Figure 4a are derived from climatological means of perpetual ENSO simulations, rather than event-based composites as in GPCP and ERA5, making direct comparison imperfect, the juxtaposition nonetheless reveals systematic differences in MJO behavior across observational and modeled frameworks.

Deleted: model

Deleted: , however

Deleted: during

Deleted: regarding

Deleted: It appears to stem from a combination of

Deleted: underestimated

Deleted: and overestimated relative to

Commented [de25]: shouldn't say this because observed composites dont run with enso forcing scaling. Using underestimate and overestimate isn't accurate

Deleted: ed

Deleted: Taken together, Figures 3 and 4 suggest that MJO periodicity tends to shorten during El Niño and lengthen during La Niña. The robustness of this relationship is further assessed using Pohl and Matthews (2007) MJO statistics, including MJO lifetime, summarized in Table 2.

EC-EARTH3.3	18.07	13.80	37.96 (1.25)	46.73 (2.01)	1.47	1.40
ECHAM5sh	26.20	15.87	28.59 (1.18)	42.94 (3.26)	1.43	1.38
EMAC	23.83	14.75	29.77 (0.88)	45.57 (1.93)	1.37	1.45
GISS-E2-2-G ^a	20.56	11.46	32.23 (1.87)	37.06 (3.50)	1.42	1.31
LMDz6 ^c	11.30	9.81	37.01 (2.20)	32.47 (1.69)	1.55	1.41
MIROC-AGCM-LL	23.48	19.26	30.31 (0.78)	30.90 (1.11)	1.46	1.49
MIROC-ESM	27.77	18.15	27.96 (0.57)	29.90 (1.15)	1.38	1.34
MRI-ESM2.0	21.53	16.70	35.02 (1.39)	39.35 (1.88)	1.43	1.40
WACCM5-110L	26.00	16.87	27.13 (0.77)	36.99 (1.31)	1.40	1.49

Commented [FS26]: elsewhere it is called GISS-E2-EG...I guess this is the "right" name?

Commented [de27R26]: thanks for pointing this out. yes, that is the right name (see: <https://www.wdc-climate.de/ui/cmip6?input=CMIP6.CMIP.NASA-GISS.GISS-E2-2-G>). I found some incorrect spellings of it throughout, which I have revised

3.1.5 MJO lifetime and event diversity

Based on ERA5, La Niña events are roughly nine days longer than El Niño events on average. Wei and Ren (2019) found La Niña to support both high-frequency (lifetime ~40 days) and low frequency (lifetime ~80 days) MJOs, which conceivably explains the much larger ERA5 lifetime standard errors during La Niña compared with El Niño. Strikingly, the difference in lifetime and its standard error between ENSO phases is nearly ubiquitous across the models. With the exception of LMDz6, La Niña lifetimes are between 0.59 (MIROC-AGCM-LL) and 15.8 (EMAC) days longer than El Niño lifetimes. Models in similar families, for instance ECHAM5sh and EMAC as well as MIROC-AGCM-LL and MIROC-ESM, typically have similar magnitude differences in their Pohl and Matthews (2007) statistics between ENSO phases. All models simulate more MJO events during El Niño, which is consistent with ERA5, however the difference in the number of events between ENSO phases is generally larger in the models than in ERA5. MJO amplitude is only marginally larger during La Niña based on ERA5 whereas six of the nine models have larger amplitudes during El Niño.

Analyzing MJO diversity offers further insight into its propagation characteristics. ~~It~~ means clustering of empirical OLR Hovmöller diagrams reveals four dominant archetypes: standing, jumping, slow, and fast propagating MJOs (Wang et al. 2019). Associated SST composites show standing MJOs tend to coincide with La Niña, fast MJOs with El Niño, while jumping and slow events show no clear ENSO linkage (Back et al. 2024). The experimental design allows us to test whether certain archetypes become more robust under persistent ENSO forcing. Fast and slow events can occur during either ENSO phase (Yadav and Straus 2017), suggesting some sensitivity of the established archetype-ENSO associations to internal variability. Figure 5 lists the number of each archetype's events simulated by each model (at the base of each bar). ~~Four~~ of seven models produce more standing events during La Niña and four models produce more jumping events during El Niño, results that do not indicate a consistent ENSO dependence. In contrast, slow and fast MJOs are modestly more frequent in El Niño simulations for six of seven models.

Formatted: Font: 10 pt

Formatted: Line spacing: 1.5 lines

Deleted: Z

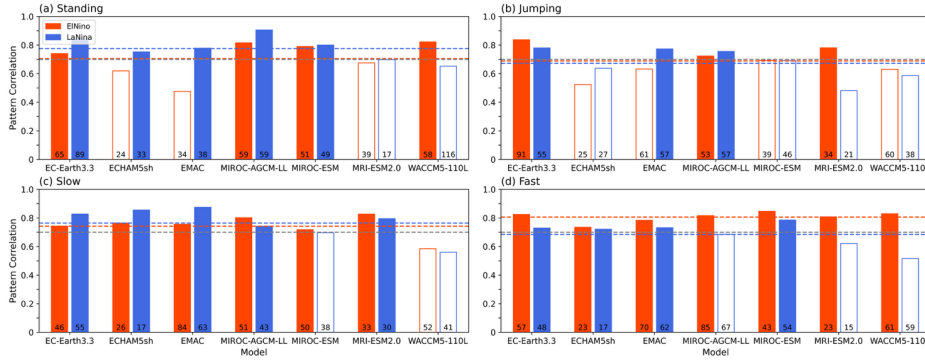
Deleted: K

Deleted: Standing and jumping MJOs occur with similar frequency across ENSO phases, with f

Deleted: producing

Deleted: producing

549
550



551
552
553
554
555
556
557
558
559
560
561
562
563
564
565
566
567
568
569
570
571
572
573
574

Figure 5: Pattern correlations between the ERA5 and simulated time-longitude (Hovmöller) 10°S-10°N convective OLR anomaly composites ($OLR < -5 \text{ W/m}^2$) corresponding to each of the four k -means clusters MJO archetypes defined in Wang et al. (2019). Multi-model average El Niño and La Niña correlations are shown by red and blue dashed lines, respectively. The gray dashed line marked at a correlation of 0.7 is a heuristic threshold (Back et al. 2024) to decide when a particular model’s MJO archetype is well captured by a model and bars are shaded in red or blue when correlation exceeds this threshold. Number of events is printed at the bottom of each bar.

To assess how closely model archetypes resemble those in reanalysis, we calculate pattern correlations between ERA5 and model time-longitude tropical OLR anomaly composites for each cluster. This evaluates how well models capture observed MJO archetypes and whether representation improves under ENSO forcing. Prior multi-model studies (Back et al. 2024) suggest a pattern correlation of 0.7 as a threshold for distinguishing well-simulated OLR Hovmöllers. For the standing MJO (Fig. 5a), five of 14 models fall below this threshold and are shaded white. Although roughly a third of simulations poorly represent the standing cluster, model skill improves during La Niña, with the multi-model mean correlation exceeding the El Niño value by 0.09. For jumping MJOs (Fig. 5b), correlations fall below 0.7 in over half the models, indicating widespread difficulty in simulating this archetype. As jumping MJOs are not thought to be ENSO-sensitive, they are not analyzed further.

Studies suggest slowly propagating MJOs often coincide with La Niña, though the associated SST pattern is weak and statistically insignificant (Wang et al. 2019; Back et al. 2024). Similarly, model skill is slightly higher in La Niña simulations, but likely indistinguishable from El Niño (Fig. 5c). In contrast, fast MJOs are better represented in every El Niño simulation, with the multi-model mean correlation exceeding the La Niña mean by 0.11 (Fig. 5d). In summary, model skill in representing fast and standing MJOs tends to be higher during El Niño and La Niña simulations, respectively, and models simulate a modestly higher number of fast events in their El Niño simulation.

Commented [FS28]: this figure should be updated?
 Commented [de29R28]: Yes and it has been updated
 Deleted: K
 Deleted: , and shaded (non-shaded) bars exceed (fall beneath) these multi-model means

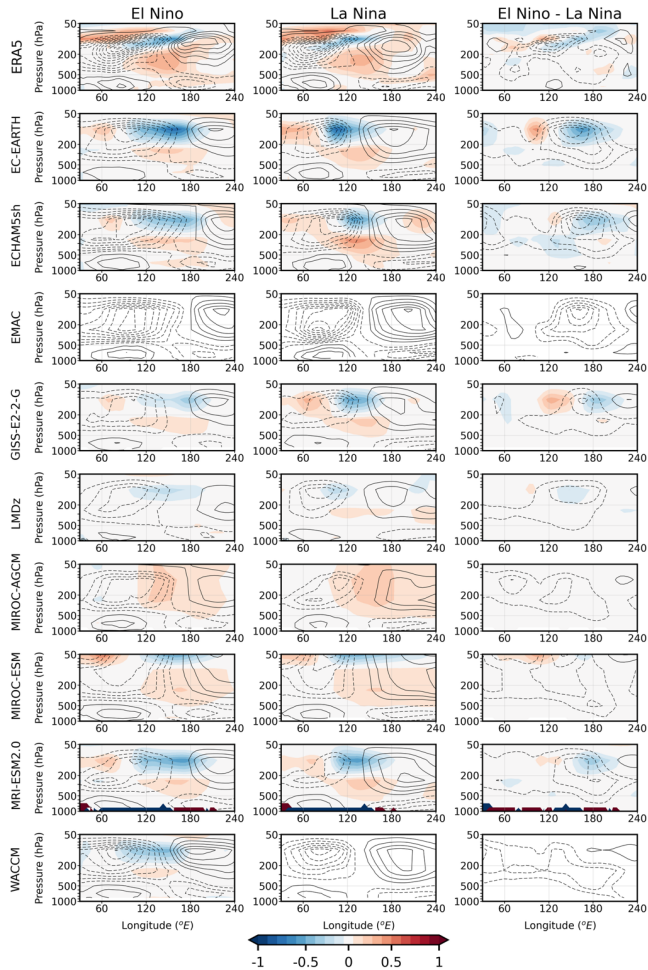
Commented [de30]: transition here

578 **3.1.6 MJO vertical structure and ENSO dependence**

579 The vertical structure of the MJO differs between slow and fast propagating events (Wang et al. 2019). To consider this
580 further, we regress the latitudinally averaged 10°S-10°N zonal wind and temperature from ERA5 and the models onto their
581 phase 3/4 RMM indices as in Hendon and Abhik (2018) and form pressure-longitude cross-sections (Figure 6). Phases 3/4,
582 when the MJO convection is over the western Maritime Continent, are of interest because ENSO modulates the low-
583 frequency circulation here through its effect on the Walker Circulation, giving it a pathway to influence MJO propagation
584 (Sun et al. 2019; Suematsu and Miura 2022). Irrespective of the ENSO phase, the MJO in ERA5 exhibits a quadrupole
585 structure in zonal wind, all of which is centered around a tropospheric warming at 140°E that peaks in amplitude near 300
586 hPa (cf. Jiang et al. 2015).

Formatted: Left

Formatted: Font: Bold



588

589 **Figure 6: Pressure-longitude cross-sections of the 10°S-10°N zonal wind and temperature regressed onto the Phase 3/4 RMMs as in**
 590 **Hendon and Abhik (2018). Black contours show zonal wind (intervals of +/- 0.5, 1.5, 2.5 m/s...) and temperature is shaded between**
 591 **-1 and 1 °C. EMAC is missing temperature and we omit WACCM's La Niña temperature due to a conspicuous artifact.**

592

593 Although the ERA5 El Niño and La Niña composites are similar overall, subtracting the two reveals that they differ due to the

594 El Niño composite including a stronger Kelvin wave, evidenced by the stronger tropospheric easterlies to the east of MJO

595 convection (cf. Fig. 2). In addition, the composites reveals a dry Kelvin wave signature, its characteristic features being a cold
596 cap temperature anomaly in the UTLS, which is slightly out of phase with easterly zonal wind anomalies, all of which tilt
597 eastward with increasing height above ~200 hPa and westward with increasing height below (Straub and Kiladis 2002; Kim
598 et al. 2013; Yuni et al. 2019; Nakamura and Takayabu 2022). Judging by the longitude of the ERA5 100 hPa cold cap maximas,
599 the dry Kelvin wave embedded in the composite El Niño MJO is shifted further east compared to its La Niña equivalent.

Deleted: .

601 Consistent with recent studies, the surface easterlies positioned east of the MJO convection are indeed stronger during El Niño
602 in reanalysis (Wang et al. 2019; Wei and Ren 2019). We attribute the amplification of these easterlies to the Kelvin wave's
603 signature in wind, which better bridges the MJO lower tropospheric easterlies over the Pacific with the upper tropospheric
604 easterly outflow over the Indian Ocean; compare the 500 hPa zonal winds at 150°E between El Niño and La Niña. This
605 enhanced continuity of the MJO easterlies during El Niño is a robust feature amongst the models and is particularly clear in
606 the El Niño minus La Niña composites of EC-EARTH3.3, ECHAM5sh, MIROC-AGCM-LL, MIROC-ESM and MRI-
607 ESM2.0.

609 It is also possible that the amplification of the equatorial Rossby wave during La Niña (cf. Figure 2) projects onto the MJO's
610 vertical structure. These waves (when located in the eastern hemisphere) have a first baroclinic structure in zonal wind that
611 consists of low-level westerlies and upper-level easterlies (Kiladis et al. 2009; Yuni et al. 2019; Nakamura and Takayabu
612 2022). Following from the robust amplification of the equatorial Rossby wave across the models during La Niña, it was
613 hypothesized that the low-level westerlies west of the MJO convection would be stronger during La Niña than El Niño like in
614 Wei and Ren (2019). This does not appear to be the case though and no first baroclinic zonal wind structure stands out in the
615 El Niño minus La Niña composites. The signal of the equatorial Rossby wave does, however, appear to be visible in the
616 temperature field. These waves are associated with a mid to upper tropospheric warming that is centered around 300 hPa
617 (Kiladis et al. 2009, Fig. 18c). This region of the upper troposphere is warmer in all of the La Niña simulations, with the
618 exception of MIROC-ESM in which the warming is marginally stronger in the El Niño composite.

Deleted: The vertical structure of the MJO zonal wind anomalies is more baroclinic during La Niña. This may be attributed to a weaker and slower propagating Kelvin wave during La Niña. However, i

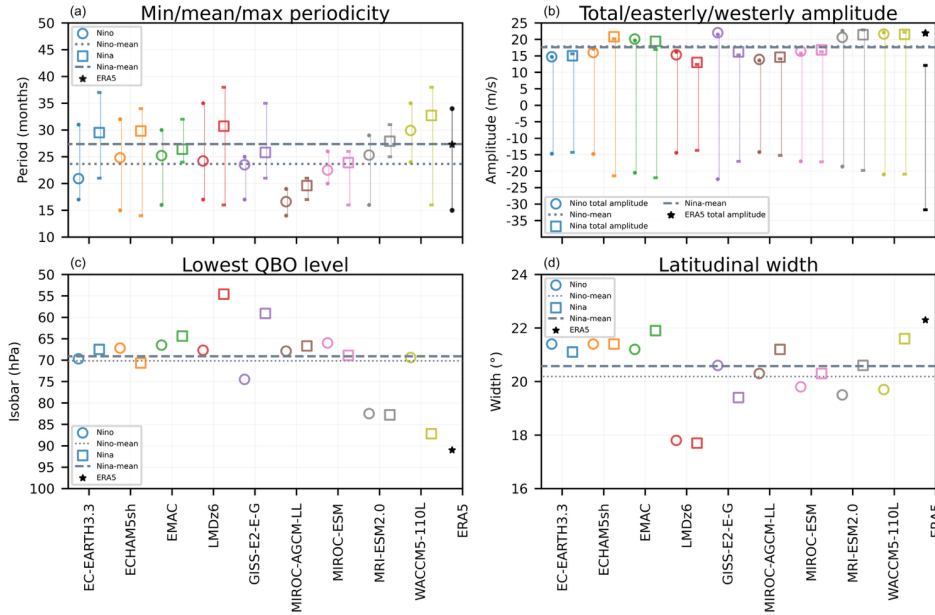
Deleted: For instance, similar to the western portion of the phase 3/4 MJO winds,

Deleted: t

620 3.2 The lack of QBO-MJO interaction

621 The results in the previous section indicate that ENSO modulates the MJO's propagation, promoting faster MJOs during El
622 Niño and the opposite during La Niña. However, it is possible that aliased signals from the spontaneously generated QBOs are
623 embedded in the aforementioned results. Therefore, in this section we look for evidence of QBO-MJO interaction. As a first
624 step, the representation of the QBO is documented using previously defined metrics, with a specific interest in quantifying the
625 "lowest level" that the QBO descends to in the lower stratosphere. Insufficient descent is a known bias, which may hinder the
626 QBO from modulating other potentially important variables near the tropopause such as temperature (Richter et al. 2020; Kim
627 et al. 2020). Similar to Schenzinger et al. (2017), the lowest level that QBO reaches is found by averaging the QBO Fourier

636 amplitude (see Methods) over 5°S-5°N, identifying the maximum amplitude (fixed at 20 hPa here), and then finding the isobar
 637 in the lower stratosphere where the amplitude equals 10% of the maximum.
 638



639 **Figure 7:** Periodicity, amplitude, lowest level of descent, and latitudinal width of the QBO in El Niño (circles) and La Niña (squares)
 640 simulations. (a) mean periodicity, where whiskers extend to the minimum and maximum period, El Niño mean is dotted, La Niña
 641 mean is dashed, and ERA5 is shown in black. (b) circles and squares show total amplitudes (“TT amplitude” from Richter et al.
 642 2020), tops of whiskers show westerly amplitudes, and bottoms of whiskers show easterly amplitudes. (c) lowest isobar the QBO
 643 descends to, the level at which the QBO Fourier amplitude falls to 10% of its maximum. (d) latitudinal width of QBO, full width at
 644 half amplitude maximum of a Gaussian fit to the QBO Fourier amplitude
 645

646
 647 The QBO descends to 92.2 hPa in ERA5 (Fig. 7c). Of the simulated QBOs, the majority do not reach beneath 70 hPa, indicating
 648 that they are likely too high in altitude to influence the tropical atmosphere beneath 100 hPa as observed (Tegtmeier et al.
 649 2020). One outlier is the WACCM5-110L’s La Niña simulation whose lowest isobar of 87 hPa is fairly similar to the ERA5
 650 benchmark. Nonetheless, sensitivity tests with this simulation in which MJO amplitude is computed as a function of lower
 651 stratospheric QBO phase reveals its MJO to be insensitive to the QBO in the observed way (not shown), which may also be



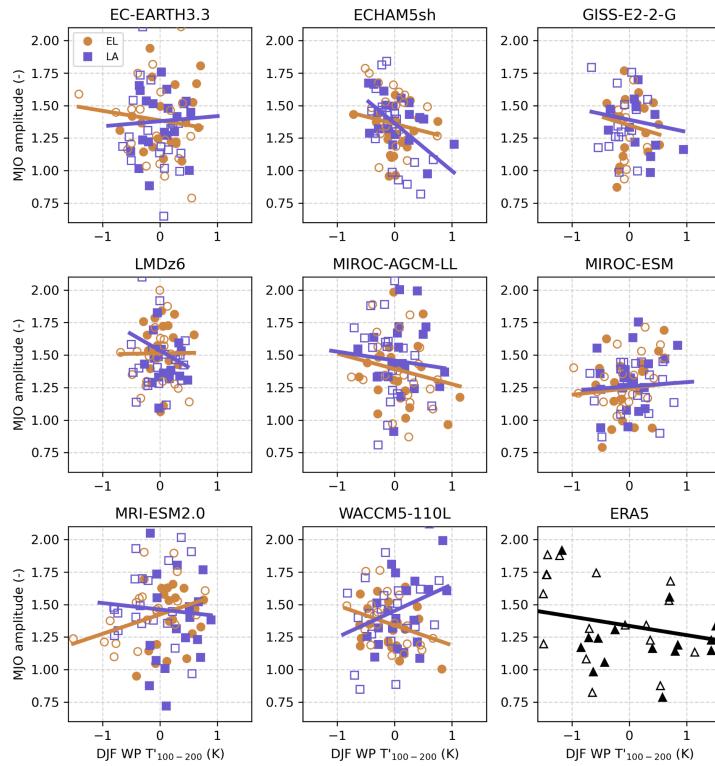
Commented [FS31]: substituted by Fig 7?

Commented [de32R31]: Yes

652 attributable to the weak MJO signal in the model. ENSO phase does not have consistent effects on what lowest isobar a given
653 model's QBO reaches. For example, GISS-E2-2-G and LMDz6 favor much stronger descent of the QBO into the lower
654 stratosphere during El Niño whereas WACCM5-110L's ENSO simulations reflect a strong opposite signed response.

655
656 QBO periodicity varies systematically with ENSO phase in these simulations, being shorter during La Niña and longer during
657 El Niño (Fig. 7a); see Kawatani et al. (2025) for a detailed analysis of this result. However, none of the QBO spatial metrics
658 exhibit consistent ENSO-phase dependence across models. For example, total QBO amplitude is marginally stronger during
659 La Niña in five of the nine models (Fig. 7b). El Niño and La Niña total QBO amplitudes differ by less than 1 m/s for all models
660 except ECHAM5sh, GISS-E2-2-G, and LMDz6. ECHAM5sh favors a stronger QBO amplitude during La Niña, owing to
661 intensified QBO easterlies and westerlies during this ENSO phase. Conversely, GISS-E2-2-G, and LMDz6 favor stronger
662 easterly, westerly, and total QBO amplitudes during El Niño. Of the 12 simulations corresponding to the six other models, EC-
663 EARTH3.3, EMAC, MIROC-AGCM-LL, MIROC-ESM, MRI-ESM2.0, and WACCM5-110L, the magnitude of their easterly
664 and westerly QBO amplitudes is stronger during La Niña in eight of the 12 simulations. Although the models ubiquitously
665 underestimate the latitudinal extent of the QBOs relative to ERA5, six of nine models have wider QBO latitudinal extents
666 during La Niña (Fig. 7d). This may be noteworthy because the boreal winter polar stratospheric wind response to the QBO is
667 stronger when the QBO is wider (Hansen et al. 2013) and there is a preference for this teleconnection to happen during La
668 Niña over the observed record (Kumar et al. 2022).

669
670



671 **Figure 8:** Scatter plot of warm-pool averaged (10°S - 10°N , 45°E - 180°E) tropopause stability anomalies (100 hPa minus 200 hPa
 672 temperature) versus December-February MJO amplitude. Lines represent the slope of the regression line during El Niño (orange)
 673 or La Niña (purple). Easterly and westerly QBO phases, which are delineated by the sign of the December-February 5°S - 5°N 50 hPa
 674 zonal mean zonal-wind, are denoted by open and filled markers, respectively.
 675
 676

677 While the aforementioned QBO metrics help to broadly characterize the form of each model's QBO, they are non-time-varying
 678 quantities and have less value for better understanding seasonal phenomena such as the predominantly boreal winter QBO-
 679 MJO interaction. To incorporate the effects of seasonality, scatterplots of December-February warm-pool averaged tropopause
 680 stability versus December-February MJO amplitude are made as a function of QBO phase for each of the simulations
 681 (Klotzbach et al. 2019). MJO amplitude is expected to increase as tropopause stability decreases (Son et al. 2017; Klotzbach
 682 et al. 2019), as is apparent based on ERA5 (Fig. 8). This metric is relevant for considering QBO-MJO coupling because the
 683 QBO's effect on lower stratospheric stability (e.g., Densmore et al. 2019) is one of the suspected physical mechanisms coupling

Commented [FS33]: this would become Fig 8 if we change the previous Table to a figure

684 the QBO and MJO. In general, the models do not reproduce the observed inverse relation between MJO amplitude and 100-
685 200 hPa stability and stratifying the results either by ENSO phase or QBO phase does not change this. The linear response of
686 the MJO amplitude to the tropopause stability, which is negative in observations, does not change consistently with the ENSO
687 phase. It is worth noting that the mean DJF stability in the models is generally close to that of ERA5 (-28.7 K) except for the
688 GISS model, which showcases a smaller gradient (-23.3 K), and all models appear to underestimate its interannual variability,
689 as evident by the smaller range compared to ERA5 (recall however that imposed SSTs do not vary interannually). Furthermore,
690 the stratification by QBO phase (with EQBO associated with lower stability values, and vice versa for the WQBO) is also
691 small or absent in models, possibly due to a limited influence of the QBO at tropopause heights (Serva et al., 2022). Further
692 sensitivity tests were done to see if the model QBOs simulate a QBO-MJO amplitude relationship when the MJO is in a
693 particular phase (e.g., Lim and Son 2020; Lawrence et al. 2023); no systematic effect was detected (not shown).

MJO Activity (OLR σ)

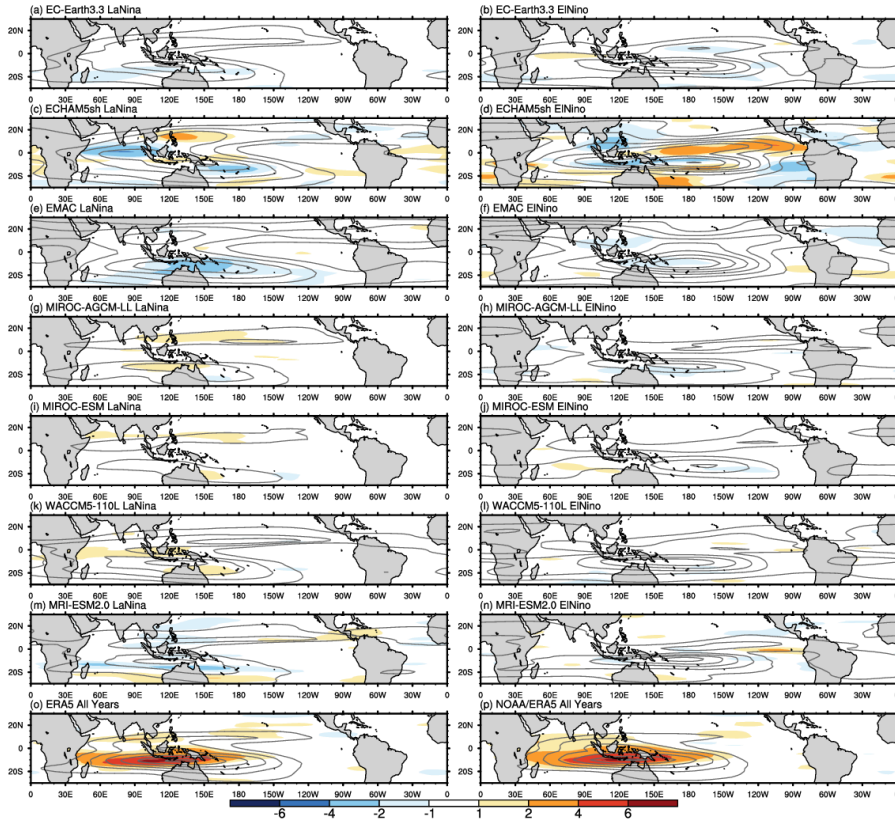


Figure 9: Gray contours show the MJO activity defined as the standard deviation of MJO-filtered OLR for each model and ENSO phase, as well as for ERA5 OLR (9o) and NOAA OLR (9n). The color-filled contours show the MJO-QBO relationship as the difference in MJO activity for the eastward minus westward 50 hPa QBO phases for each model and using the ERA5 wind in 9o and 9n.

To further evaluate the representation of QBO-MJO coupling in the models, Figure 9 presents the effect of QBO phase on MJO activity (see Methods). As shown in previous studies (e.g., Kim et al. 2020), the models do not capture the observed

Deleted: (6n)

Commented [FS34]: at which level? It is interesting to note that ECHMA5sh QBO in EL tends to stall - similar thing happening in GISS during LA. check Fig 2 <https://egusphere.copernicus.org/preprints/2024/egusphere-2024-3270/egusphere-2024-3270.pdf>

Commented [FS35R34]: but since GISS is missing (I guess because it has no OLR) I think we can't conclude much

Commented [de36R34]: added 50 hPa as level. See Methods too. We now have two mentions (L605, L647) of basic state wind biases associated with the QBO

703 QBO-MJO relationship, which has maximum signal over the maritime continent region (Fig. 9m) illustrating the enhancement
704 of MJO activity during easterly QBO phase. With La Niña forcing, MIROC-AGCM-LL and WACCM5-110L show a weak
705 positive signal over the Maritime Continent (Fig. 9g, k), however EC-EARTH3.3, ECHAM5sh, and EMAC exhibit rather
706 different responses. In MIROC models, the MJO activity is further shifted off-equator, possibly hampering any QBO control
707 on MJO convection. No change in the MJO activity by QBO phase is evident in the El Niño simulations either, except for
708 some negative signal in the central and eastern Pacific in ECHAM5sh, which may be due to an irregular QBO in this experiment
709 (Kawatani et al., 2025). There is, however, a clear eastward shift of the MJO activity towards the Pacific during El Niño,
710 corroborating the observational work of Kessler (2001) and the climate model based study of Tam and Lau (2005).

711 4 Discussion and conclusions

712 The observed interannual variability of the MJO is influenced by multiple parts of the climate system. Due to their impact on
713 the tropical troposphere and prominent fluctuations at interannual timescales, ENSO and the QBO are known drivers of the
714 MJO's year to year variability, however it is difficult to definitively isolate their influence on the MJO because of how short
715 and noisy the observational record is (Randall et al. 2023). Building on previous work, our aim here is to evaluate the extent
716 to which model behavior is consistent with previously reported ENSO-MJO relationships by analyzing the representation of
717 the MJO in nine climate models forced by prescribed perpetual El Niño and La Niña conditions, each with a spontaneously
718 generated QBO. While the imposed SST anomalies represent an upper bound for the observed record, they are relevant given
719 the projected intensity increase of ENSO extremes.

720
721 Although the models exhibit difficulties simulating the MJO, several previously reported effects of the ENSO phase on the
722 MJO are corroborated by this coordinated set of experiments. These effects include faster propagation of the MJO during El
723 Niño versus slower propagation during La Niña, manifesting as shorter and longer lifetimes, respectively, stronger amplitude
724 of the MJO during El Niño, and east-west shifting of the MJO timescale variance towards the east Pacific during El Niño and
725 towards the west Pacific and Indian Ocean during La Niña.

726
727 It is likely that the high-amplitude SST forcings used here, particularly the amplified El Niño forcing, contribute to the
728 magnitude of these ENSO associated MJO changes, consistent with prior work linking exceptionally warm Pacific SSTs to
729 enhanced or farther-east MJO propagation (e.g., Marshall et al. 2016). To assess this sensitivity to ENSO amplitude, [in one](#)
730 [analysis](#) we compare a broad measure of MJO quality and propagation, the MJO E/W ratio, between the perpetual ENSO
731 simulations and each model's 1979–2009 AMIP simulations, [the latter of](#) which are more representative of typical ENSO
732 amplitudes. Across models, [the amplified](#) El Niño forcing increases the E/W ratio [relative to La Niña](#), [shifting](#) it toward the
733 upper tail of the AMIP-based internal variability distribution [and](#), [indicating more robust eastward MJO propagation](#). [All](#)
734 perpetual ENSO E/W [still](#) ratios remain within the spectrum of their AMIP-based values, underscoring that the modeled

~~Deleted: often pushing~~

~~Deleted: ,~~

~~Deleted: whereas many La Niña simulations produce ratios near unity~~

~~Deleted: Notably, a~~

740 responses, while produced by extreme forcings, are consistent with how the MJO behaves under normal SSTs. For GPCP and
741 ERA5, however, their composite El Niño and La Niña MJO E/W ratios sit centrally within the distribution of sampling
742 variability (Fig. 4a), which supports Slingo et al. (1999) and Hendon et al. (1999)'s conclusion that ENSO does not strongly
743 modulate seasonal-mean MJO activity. Thus, the ENSO-MJO sensitivity expressed in the models is less clearly present in
744 observations, implying either reduced sensitivity in nature or an exaggerated response to the imposed SST anomalies.

745
746 Beyond the E/W ratio, other indicators of MJO activity demonstrate strong responses to ENSO forcing in these simulations,
747 differing from these studies. Hendon et al. (1999) found that increased MJO activity coincides with an increased number of
748 MJO events and enhanced intraseasonal convective activity around the Maritime Continent. While these attributes of the MJO
749 were largely insensitive to SSTs in their study, the models here unambiguously simulate more events in their perpetual El Niño
750 simulation (Table 2), which are of stronger MJO activity than their La Niña equivalents (Figure 9). We suspect that the
751 distinction between our results and previous research is related to the timescale over which the oceanic component of ENSO
752 modulates the atmosphere. Recent studies show that while the likelihood of MJO occurrence and its propagation speed are
753 only weakly correlated with tropical intraseasonally filtered SSTs, they are strongly correlated with low-frequency (e.g., > 90
754 days) SSTs (Suematsu and Miura 2018; 2022). In light of this and our use of a simplified climate system in which smoothed
755 monthly SSTs are prescribed, intraseasonal and interannual SST fluctuations are explicitly ignored, and the downward impact
756 of the MJO on intraseasonal SSTs (Zhang and Gottschalk 2002; Hendon et al. 2007; Newman et al. 2009) is not simulated, we
757 deduce that the different basic state circulations set up by the indefinite ENSO forcings enables distinct MJOs. This
758 interpretation of the low-frequency SSTs as an important modulator of the MJO aligns with studies which have attributed
759 variability in the MJO's propagation to ENSO (Wei and Ren 2019; Wang et al. 2019; Dasgupta et al. 2021; Back et al. 2024)
760 as well as studies employing climate models in which MJO propagation can be modulated by changing the horizontal gradients
761 of the background SST field (Kang et al. 2013; Jiang et al. 2020).

762
763 We note that, besides SST amplitude, the representation of MJOs in models appears to be particularly sensitive to convective
764 schemes, as discussed by Rind et al. (2020) for GISS, by Park et al. (2019) for WACCM, by Miura et al. (2012) for MIROC
765 and Holt et al. (2020) for other Phase 1 QBOi models. The impact of the convective scheme, for example, appears oversized
766 compared to horizontal resolution, which is finely resolved in EC-EARTH3.3, MIROC-AGCM-LL, MRI-ESM2.0, and
767 WACCM, none of which are exceptional at reproducing the MJO's wavenumber frequency spectra or E/W ratios. Moreover,
768 models within the same family (MIROC-based, ECHAM-based) exhibit similar MJO spectra (Fig. 2, Fig. 4), despite having
769 intra-family differences in horizontal and vertical resolution (Table 2; Holt et al. 2020, Fig. 18). As shown by Orbe et al. (2020)
770 for the WACCM and GISS models, refinement of key parameterization has potential to improve simulated MJOs.

771
772 As in the observational record, it is possible that aliasing from the QBO is superimposed on what are thought to be MJO
773 changes due to ENSO. However, we find that the climate models considered here show little evidence of QBO-MJO coupling.

Deleted: do not exceed the range of variability seen under more

Deleted: s

Commented [FS37]: do we add this?
<https://journals.ametsoc.org/view/journals/clim/33/17/jcliD190956.pdf>

Commented [de38R37]: Yes - nice addition!

777 This may be due to various factors, such as biases in the descent of the QBO, and the location and characteristics of tropical
778 convection, which appears to be less organized in some of the models compared to GPCP. While this limits our ability to
779 diagnose the mechanisms linking the QBO and MJO, it suggests that, in these experiments, the MJO changes we detect are
780 primarily driven by the ENSO forcings. Experiments with specified rather than internally generated QBO aspects can help
781 understanding the processes at play, which remain elusive (Martin et al., 2023; Huang et al. 2023). One speculative reason for
782 the missing QBO-MJO signal is the representation of upper tropospheric Kelvin waves. Observations show that during EQBO,
783 the Kelvin wave associated with the MJO penetrates higher into the lower stratosphere, coinciding with an eastward-tilting
784 cold anomaly in the UTLS (Hendon and Abhik 2018). We find a similar dry Kelvin wave signature in our ERA5 El Niño
785 minus La Niña MJO vertical structure composite, but in models, the UTLS wave structure is much more coarsely resolved
786 (Fig. 6). Such deficiencies, perhaps linked to vertical resolution (Holt et al. 2020, Fig. 18a), lower-stratospheric wind biases
787 that develop in the absence of sufficient QBO descent (Fig. 7c), or perhaps just weak MJOs, may weaken this dry Kelvin wave
788 component and, in turn, suppress QBO-MJO interaction.

790 ↓
791 Compared with the La Niña simulations, all El Niño simulations include amplified Kelvin waves whereas equatorial Rossby
792 waves intensify in the presence of perpetual La Niña conditions. Consistent with the reported relationship between the these
793 waves and the MJO (Wei and Ren 2019), all models simulate faster MJO propagation in their El Niño simulation. This is
794 further supported by the MJO diversity analysis, which reveals that models reproduce the observed fast and standing MJO
795 archetype OLR Hovmöllers well in the presence of perpetual El Niño and La Niña conditions, respectively. In addition, the
796 MJO's phase 3/4 vertical structures highlight that lower tropospheric easterlies do intensify to the east of the MJO's major
797 convection during El Niño across most models, which we interpret to result from the intensification of the Kelvin wave.

799 The strengthening of model equatorial Rossby and Kelvin waves under La Niña and El Niño forcing, respectively, is broadly
800 consistent with observational studies (Wei and Ren 2019; Wang et al. 2019), yet the striking uniformity of these responses
801 across models and underlying mechanisms are not fully understood. Both waves exhibit substantial longitudinal variation in
802 observations, and their behavior depends on multiple aspects not considered in detail here, including seasonal-mean
803 convection, ambient zonal wind, and the extent to which extratropical planetary waves can intrude into the tropics (Yang et al.
804 2023). These factors, in turn, are further shaped by the model-dependent tropospheric responses to the internally generated
805 QBOs (Naoe et al. 2025). Because these degrees of freedom are not isolated in our study, we cannot yet diagnose with
806 confidence why the models produce such consistent equatorial Rossby and Kelvin wave responses to the ENSO forcings.
807 Nevertheless, the fact that this coherence emerges despite these unconstrained influences underscores the robustness of the
808 simulated wave responses and motivates a closer examination of the waves in subsequent work.

809 While the modeled relationship between Kelvin waves, equatorial Rossby waves, and ENSO is well supported by previous
810 studies employing empirical data and reanalysis, this is the first time, to the best of our knowledge, that this relationship has

Commented [FS39]: related to spectrum shifts in wavenumber

Commented [de40R39]: Yeah, I think is valid based on Fig 2/4

Commented [FS42R41]: As a perspective, I guess we could add that improving the MJO representation seems to be important

Commented [de43R41]: I alluded to the importance of improving the MJOs in P1 and P2 of the conclusions rather than here in paragraph three (P3)

Deleted: These results highlight that the interannual variability of the MJO

Deleted: is sensitive to ENSO in several regards, in contrast with Slingo et al. (1999) and Hendon et al. (1999). These studies reported a weak simultaneous relationship between ENSO and MJO activity. Hendon et al. (1999) found that increased MJO activity coincides with an increased number of MJO events and enhanced intraseasonal convective activity around the Maritime Continent. While these attributes of the MJO were largely insensitive to SSTs in their study, the models here unambiguously simulate more events in their perpetual El Niño simulation (Table 2), which are of stronger MJO activity than their La Niña equivalents (Figure 8). We suspect that the distinction between our results and the previous research is related to the timescale over which the oceanic component of ENSO modulates the atmosphere. Recent studies show that while the likelihood of MJO occurrence and its propagation speed are only weakly correlated with tropical intraseasonally filtered SSTs, t' (... [2])

Commented [FS44]: we could mention here the studies by Yang who found substantial regional variations, which (... [3])

Commented [de45R44]: we now mention these studies, both in section 3.1 and in conclusion

Commented [FS46]: there were comment on dry waves etc....to be implemented better

Commented [de47R46]: I simply mentioned "dry kelvin wave signature" above where relevant, but don't want (... [4])

Commented [de48R46]: I did revise the text beneath Figure 6, where the reviewer made their comment, to contrast (... [5])

Commented [FS49]: I think we should add a sentence or two on why these are better than MJOs

Commented [FS50R49]: based on Holt 2020, I guess the motivation is that these are larger and somewhat less (... [6])

Commented [de51R49]: I omitted this because it's complicated. The sensitivity of MJO E/W ratios to the (... [7])

Deleted:

Deleted: ¶

Deleted: established

871 been ubiquitously affirmed by a coordinated set of climate model experiments with prescribed strong ENSO forcings. The
872 robustness of this result across models suggests that it is worthwhile considering how these wave responses to ENSO influence
873 other parts of the climate system. For instance, Kelvin waves are a source of resolved wave forcing for the QBO (Baldwin et
874 al. 2001; Taguchi 2010; Pahlavan et al. 2021) and more rapid descent of the QBO's westerly shear zones during El Niño in
875 observations has been attributed to their intensification (Das and Pan 2016). The periodicity of the QBO in the El Niño
876 simulations is in fact shorter than in the La Niña simulations across all models considered here (Kawatani et al., 2025),
877 however, the extent to which Kelvin waves are responsible for this as opposed to other waves (e.g., Kawatani et al. 2019), is
878 yet to be quantified across all of the models. The convectively coupled wave responses presented here may also be relevant
879 for better understanding of the observed ENSO diversity. El Niño events vary in type and intensity due to the influence of
880 westerly wind bursts, which introduce asymmetry and irregularity into ENSO's phase changes (Chen et al. 2015). Westerly
881 wind bursts are more frequent during the convective phases of equatorial Rossby waves and the MJO, especially strong MJOs
882 (Puy et al. 2016). Hence, the atmospheric responses to ENSO, such as the amplifications of the MJO during El Niño (Figs. 2-
883 4) and of the convectively coupled Rossby wave during La Niña, have a pathway to influence ENSO's oceanic component.

885 **Code availability**

886
887 The code used for the wavenumber-frequency analysis is publicly available through the National Center for Atmospheric
888 Research (NCAR) Command Language (NCL): <https://www.ncl.ucar.edu/Applications/mjoclivar.shtml>. A reproduction of
889 NCL's Wheeler-Kiladis (1999) routine in Python is available here: https://github.com/brianpm/wavenumber_frequency.
890 Python code, which assesses QBO morphology is available here: [https://github.com/NOAA-GFDL/MDTF-](https://github.com/NOAA-GFDL/MDTF-diagnostics/blob/main/diagnostics/stc_qbo_ens0/stc_qbo_ens0.py)
891 [diagnostics/blob/main/diagnostics/stc_qbo_ens0/stc_qbo_ens0.py](https://github.com/NOAA-GFDL/MDTF-diagnostics/blob/main/diagnostics/stc_qbo_ens0/stc_qbo_ens0.py).

893 **Data availability**

894 Storage for the QBOi multi-model data set is provided by the Centre for Environmental Data Analysis (CEDA) whose data
895 and processing service is called JASMIN. Interested users must obtain a JASMIN login account and take the necessary steps
896 to access the QBOi group workspace within JASMIN, which contains the perpetual ENSO simulations. Certain derived model
897 products (e.g., the MJO RMMs) may be made available upon request.

899 **Author contributions**

900 DE, FS, JC, SYB, CO, and JR contributed to the conceptualization of this study. DE, FS, JC, and SYB performed the data
901 analyses and produced the figures and tables. All authors contributed to the review and editing of this manuscript.

903 **Competing interests**

904 The authors declare that they have no conflict of interest.

Commented [FS52]: indeed following the reviewers I'd add here a paragraph on the (lack of) QBO MJO connection

Commented [FS53R52]: The fact that Huang stresses temperature makes me wonder if convection characteristics also matters

Commented [de54R52]: I added the Huang reference with the Martin et al. 2023 reference in Conclusions section paragraph 2. I also added speculations on the lack of QBO-MJO coupling there

Commented [FS55]: to reiterate that here ENSO is prescribed

Commented [FS56]: update if needed

905

906 **Acknowledgements**

907 [The authors appreciate the helpful suggestions and questions from two anonymous reviewers and the editor, whose](#)
 908 [involvement improved this manuscript.](#) DE was supported in part by NOAA Cooperative Agreement NA22OAR4320151 and
 909 appreciates helpful [discussions](#) with John Albers, Juliana Dias, George Kiladis, Matthew Newman, Brandon Wolding, and
 910 Amy Butler. The ECHAM5sh simulations were performed thanks to an ECMWF Special Project awarded to FS. YK[KY1]
 911 was supported by JSPS KAKENHI (JP22K18743) and the Environment Research and Technology Development Fund
 912 (JPMEERF20242001) of the Environmental Restoration and Conservation Agency provided by Ministry of the Environment
 913 of Japan. YK and SW were supported by JSPS KAKENHI (JP22H01303 and JP23K22574). SW was supported by MEXT-
 914 Program for the advanced studies of climate change projection (SENTAN) Grant Number JPMXD0722681344. [SB and SS](#)
 915 [were supported by Korea Environment Industry & Technology Institute \(KEITI\) through ‘Climate Change R&D Project for](#)
 916 [New Climate Regime.’ funded by Korea Ministry of Environment \(MOE\) \(2022003560004\).](#) NB was funded by the Met Office
 917 Climate Science for Service Partnership (CSSP) China project under the International Science Partnerships Fund (ISPF). The
 918 numerical simulations of MIROC models were performed using the Earth Simulator. The GFD-DENNOU Library and GrADS
 919 were used to draw the figures. TK and SV acknowledge support by the state of Baden-Württemberg through bwHPC. Portions
 920 of this work were supported by the National Center for Atmospheric Research (NCAR), which is a major facility sponsored
 921 by the National Science Foundation (NSF) under Cooperative Agreement 1852977. Portions of this study were supported by
 922 the Regional and Global Model Analysis (RGMA) component of the Earth and Environmental System Modeling Program of
 923 the U.S. Department of Energy’s Office of Biological and Environmental Research (BER) via NSF Interagency Agreement
 924 1844590. The authors gratefully acknowledge the UK Centre for Environmental Data Analysis for providing archival and
 925 analysis resources for the QBOi multimodel dataset.

926

927 **References**

928

929 Adler, Robert; Wang, Jian-Jian; Sapiano, Mathew; Huffman, George; Bolvin, David; Nelkin, Eric; and NOAA CDR Program
 930 (2017). Global Precipitation Climatology Project (GPCP) Climate Data Record (CDR), Version 1.3 (Daily) [1996-2022].
 931 NOAA National Centers for Environmental Information. doi:10.7289/V5RX998Z [July 2025]
 932
 933 [\[Ahn\] M.-S., Kim, D., Sperber, K. R., Kang, I.-S., Maloney, E., Waliser, D., and Hendon, H.: MJO simulation in CMIP5 climate](#)
 934 [models: MJO skill metrics and process-oriented diagnosis, Clim Dyn, 49, 4023–4045, \[3558-4\]\(https://doi.org/10.1007/s00382-017-

 935 <a href=\), 2017.](#)
 936
 937 Ahn, M., Kim, D., Kang, D., Lee, J., Sperber, K. R., Gleckler, P. J., Jiang, X., Ham, Y., and Kim, H.: MJO Propagation Across
 938 the Maritime Continent: Are CMIP6 Models Better Than CMIP5 Models?, Geophysical Research Letters, 47,
 939 e2020GL087250, <https://doi.org/10.1029/2020GL087250>, 2020.
 940
 941 Back, S.-Y., Kim, D., and Son, S.-W.: MJO Diversity in CMIP6 Models, Journal of Climate, 37, 4835–4850,
 942 <https://doi.org/10.1175/JCLI-D-23-0656.1>, 2024.

Commented [FS57]: also Amy?

Commented [de58R57]: added amy

Deleted: S.-W. Son was supported by a grant from the National Research Foundation of Korea (NRF), funded by the Korean government (MSIT) (2023R1A2C3005607).

Commented [FS59]: to do: cross-check all refs with the text before submission

Commented [FS60]: first one should be Adler of any GPCP ref

Commented [FS61R60]: please Dillon confirm the version

Commented [de62R60]: V1.3 - see thread above

946
947 Baldwin, M. P., Gray, L. J., Dunkerton, T. J., Hamilton, K., Haynes, P. H., Randel, W. J., Holton, J. R., Alexander, M. J.,
948 Hirota, I., Horinouchi, T., Jones, D. B. A., Kimmersley, J. S., Marquardt, C., Sato, K., and Takahashi, M.: The quasi-biennial
949 oscillation, *Reviews of Geophysics*, 39, 179–229, <https://doi.org/10.1029/1999RG000073>, 2001.
950
951 Bechtold, P., Semane, N., Lopez, P., Chaboureaud, J.-P., Beljaars, A., and Bormann, N.: Representing Equilibrium and
952 Nonequilibrium Convection in Large-Scale Models, *Journal of the Atmospheric Sciences*, 71, 734–753,
953 <https://doi.org/10.1175/JAS-D-13-0163.1>, 2014.
954
955 Berrington, A. H., Sakaeda, N., Dias, J., and Kiladis, G. N.: Relationships Between the Eastward Propagation of the Madden-
956 Julian Oscillation and Its Circulation Structure, *JGR Atmospheres*, 127, e2021JD035806,
957 <https://doi.org/10.1029/2021JD035806>, 2022.
958
959 Bushell, A. C., Anstey, J. A., Butchart, N., Kawatani, Y., Osprey, S. M., Richter, J. H., Serva, F., Braesicke, P., Cagnazzo, C.,
960 Chen, C.-C., Chun, H.-Y., Garcia, R. R., Gray, L. J., Hamilton, K., Kerzenmacher, T., Kim, Y.-H., Lott, F., McLandress, C.,
961 Naoe, H., Scinocca, J., Smith, A. K., Stockdale, T. N., Versick, S., Watanabe, S., Yoshida, K., and Yukimoto, S.: Evaluation
962 of the Quasi-Biennial Oscillation in global climate models for the SPARC QBO-initiative, *Quart J Royal Meteor Soc*, 148,
963 1459–1489, <https://doi.org/10.1002/qj.3765>, 2022.
964
965 Butchart, N., Anstey, J. A., Hamilton, K., Osprey, S., McLandress, C., Bushell, A. C., Kawatani, Y., Kim, Y.-H., Lott, F.,
966 Scinocca, J., Stockdale, T. N., Andrews, M., Bellprat, O., Braesicke, P., Cagnazzo, C., Chen, C.-C., Chun, H.-Y., Dobrynin,
967 M., Garcia, R. R., Garcia-Serrano, J., Gray, L. J., Holt, L., Kerzenmacher, T., Naoe, H., Pohlmann, H., Richter, J. H., Scaife,
968 A. A., Schenzinger, V., Serva, F., Versick, S., Watanabe, S., Yoshida, K., and Yukimoto, S.: Overview of experiment design
969 and comparison of models participating in phase 1 of the SPARC Quasi-Biennial Oscillation initiative (QBOi), *Geosci. Model*
970 *Dev.*, 11, 1009–1032, <https://doi.org/10.5194/gmd-11-1009-2018>, 2018.
971
972 Chen, D., Lian, T., Fu, C., Cane, M. A., Tang, Y., Murtugudde, R., Song, X., Wu, Q., and Zhou, L.: Strong influence of
973 westerly wind bursts on El Niño diversity, *Nature Geosci*, 8, 339–345, <https://doi.org/10.1038/ngeo2399>, 2015.
974
975 Chikira, M. and Sugiyama, M.: A Cumulus Parameterization with State-Dependent Entrainment Rate. Part I: Description and
976 Sensitivity to Temperature and Humidity Profiles, *Journal of the Atmospheric Sciences*, 67, 2171–2193,
977 <https://doi.org/10.1175/2010JAS3316.1>, 2010.
978
979 Das, U. and Pan, C. J.: Equatorial atmospheric Kelvin waves during El Niño episodes and their effect on stratospheric QBO,
980 *Science of The Total Environment*, 544, 908–918, <https://doi.org/10.1016/j.scitotenv.2015.12.009>, 2016.
981
982 Dasgupta, P., Roxy, M. K., Chattopadhyay, R., Naidu, C. V., and Metya, A.: Interannual variability of the frequency of MJO
983 phases and its association with two types of ENSO, *Sci Rep*, 11, 11541, <https://doi.org/10.1038/s41598-021-91060-2>, 2021.
984
985 Densmore, C. R., Sanabia, E. R., and Barrett, B. S.: QBO Influence on MJO Amplitude over the Maritime Continent: Physical
986 Mechanisms and Seasonality, *Monthly Weather Review*, 147, 389–406, <https://doi.org/10.1175/MWR-D-18-0158.1>, 2019.
987
988 Emanuel, K. A.: A Scheme for Representing Cumulus Convection in Large-Scale Models, *J. Atmos. Sci.*, 48, 2313–2329,
989 [https://doi.org/10.1175/1520-0469\(1991\)048<2313:ASFRCC>2.0.CO;2](https://doi.org/10.1175/1520-0469(1991)048<2313:ASFRCC>2.0.CO;2), 1991.
990
991 Emori, S., Nozawa, T., Numaguti, A., and Uno, I.: Importance of Cumulus Parameterization for Precipitation Simulation over
992 East Asia in June., *Journal of the Meteorological Society of Japan*, 79, 939–947, <https://doi.org/10.2151/jmsj.79.939>, 2001.
993
994 Fernandes, L. G. and Grimm, A. M.: ENSO Modulation of Global MJO and Its Impacts on South America, *Journal of Climate*,
995 36, 7715–7738, <https://doi.org/10.1175/JCLI-D-22-0781.1>, 2023.

996
997 Gehne, M., Hamill, T. M., Kiladis, G. N., and Trenberth, K. E.: Comparison of Global Precipitation Estimates across a Range
998 of Temporal and Spatial Scales. *Journal of Climate*, 29(21), 7773–7795. <https://doi.org/10.1175/JCLI-D-15-0618.1>, 2016.
999

1000 Hendon, H. H. and Abhik, S.: Differences in Vertical Structure of the Madden-Julian Oscillation Associated With the Quasi-
1001 Biennial Oscillation, *Geophysical Research Letters*, 45, 4419–4428, <https://doi.org/10.1029/2018GL077207>, 2018.
1002

1003 Ham, S. and Hong, S.-Y.: Sensitivity of simulated intraseasonal oscillation to four convective parameterization schemes in a
1004 coupled climate model, *Asia-Pacific J Atmos Sci*, 49, 483–496, <https://doi.org/10.1007/s13143-013-0043-9>, 2013.
1005

1006 Hansen, F., Matthes, K., and Gray, L. J.: Sensitivity of stratospheric dynamics and chemistry to QBO nudging width in the
1007 chemistry–climate model WACCM, *JGR Atmospheres*, 118, <https://doi.org/10.1002/jgrd.50812>, 2013.
1008

1009 Hendon, H. H. and Salby, M. L.: The Life Cycle of the Madden–Julian Oscillation, *J. Atmos. Sci.*, 51, 2225–2237,
1010 [https://doi.org/10.1175/1520-0469\(1994\)051<2225:TLCO TM>2.0.CO;2](https://doi.org/10.1175/1520-0469(1994)051<2225:TLCO TM>2.0.CO;2), 1994.
1011

1012 Hendon, H. H., Zhang, C., and Glick, J. D.: Interannual Variation of the Madden–Julian Oscillation during Austral Summer,
1013 *J. Climate*, 12, 2538–2550, [https://doi.org/10.1175/1520-0442\(1999\)012<2538:IVOTMJ>2.0.CO;2](https://doi.org/10.1175/1520-0442(1999)012<2538:IVOTMJ>2.0.CO;2), 1999.
1014

1015 Hendon, H. H., Wheeler, M. C., and Zhang, C.: Seasonal Dependence of the MJO–ENSO Relationship, *Journal of Climate*,
1016 20, 531–543, <https://doi.org/10.1175/JCLI4003.1>, 2007.
1017

1018 Henley, B. J., Gergis, J., Karoly, D. J., Power, S., Kennedy, J., and Folland, C. K.: A Tripole Index for the Interdecadal Pacific
1019 Oscillation, *Clim Dyn*, 45, 3077–3090, <https://doi.org/10.1007/s00382-015-2525-1>, 2015.
1020

1021 Hourdin, F., Grandpeix, J.-Y., Rio, C., Bony, S., Jam, A., Cheruy, F., Rochetin, N., Fairhead, L., Idelkadi, A., Musat, I.,
1022 Dufresne, J.-L., Lahellec, A., Lefebvre, M.-P., and Roehrig, R.: LMDZ5B: the atmospheric component of the IPSL climate
1023 model with revisited parameterizations for clouds and convection, *Clim Dyn*, 40, 2193–2222, <https://doi.org/10.1007/s00382-012-1343-y>, 2013.
1024

1025

1026 Huang, K., Richter, J. H., and Pegion, K. V.: Captured QBO-MJO Connection in a Subseasonal Prediction System,
1027 *Geophysical Research Letters*, 50, e2022GL102648, <https://doi.org/10.1029/2022GL102648>, 2023.
1028

1029 Huffman, G.J., R.F. Adler, M. Morrissey, D.T. Bolvin, S. Curtis, R. Joyce, B McGavock, J. Susskind: Global Precipitation at
1030 One-Degree Daily Resolution from Multi-Satellite Observations. *J. Hydrometeor.*, 2(1), 36-50, doi.org/10.1175/1525-
1031 7541(2001)002<0036:GPAODD>2.0.CO;2, 2001
1032

1033 Jiang, X., Waliser, D. E., Xavier, P. K., Petch, J., Klingaman, N. P., Woolnough, S. J., Guan, B., Bellon, G., Crueger, T.,
1034 DeMott, C., Hannay, C., Lin, H., Hu, W., Kim, D., Lappen, C., Lu, M., Ma, H., Miyakawa, T., Ridout, J. A., Schubert, S. D.,
1035 Scinocca, J., Seo, K., Shindo, E., Song, X., Stan, C., Tseng, W., Wang, W., Wu, T., Wu, X., Wyser, K., Zhang, G. J., and Zhu,
1036 H.: Vertical structure and physical processes of the Madden-Julian oscillation: Exploring key model physics in climate
1037 simulations, *JGR Atmospheres*, 120, 4718–4748, <https://doi.org/10.1002/2014JD022375>, 2015.
1038

1039 Jiang, X., Maloney, E., and Su, H.: Large-scale controls of propagation of the Madden-Julian Oscillation, *npj Clim Atmos Sci*,
1040 3, 29, <https://doi.org/10.1038/s41612-020-00134-x>, 2020.
1041

1042 Jin, D., D. Kim, S.-W. Son, and L. Oreopoulos, 2023: QBO deepens MJO convection, *Nature Communications*, 14, 4088,
1043 <https://doi.org/10.1038/s41467-023-39465-7>
1044

1045 Kang, I.-S., Liu, F., Ahn, M.-S., Yang, Y.-M., and Wang, B.: The Role of SST Structure in Convectively Coupled Kelvin–
1046 Rossby Waves and Its Implications for MJO Formation, *Journal of Climate*, 26, 5915–5930, <https://doi.org/10.1175/JCLI-D-12-00303.1>, 2013.

1047
1048
1049 Kawatani, Y., Hamilton, K., Sato, K., Dunkerton, T. J., Watanabe, S., and Kikuchi, K.: ENSO Modulation of the QBO: Results
1050 from MIROC Models with and without Nonorographic Gravity Wave Parameterization, *Journal of the Atmospheric Sciences*,
1051 76, 3893–3917, <https://doi.org/10.1175/JAS-D-19-0163.1>, 2019.

1052
1053
1054 [↓
1055 Kawatani, Y., Hamilton, K., Watanabe, S., Taguchi, M., Serva, F., Anstey, J. A., Richter, J. H., Butchart, N., Orbe, C., Osprey,
1056 S. M., Naoe, H., Elsbury, D., Chen, C.-C., García-Serrano, J., Glanville, A., Kerzenmacher, T., Lott, F., Palmeiro, F. M., Park,
1057 M., Versick, S., and Yoshida, K.: QBO El Niño–Southern Oscillation experiments: overview of the experimental design and
1058 ENSO modulation of the QBO. *Weather Clim. Dynam.*, 6, 1045–1073, <https://doi.org/10.5194/wcd-6-1045-2025>, 2025.](https://doi.org/10.5194/wcd-6-1045-2025)

1059 Kelley, M., Schmidt, G. A., Nazarenko, L. S., Bauer, S. E., Ruedy, R., Russell, G. L., Ackerman, A. S., Aleinov, I., Bauer, M.,
1060 Bleck, R., Canuto, V., Cesana, G., Cheng, Y., Clune, T. L., Cook, B. I., Cruz, C. A., Del Genio, A. D., Elsaesser, G. S.,
1061 Faluvegi, G., Kiang, N. Y., Kim, D., Laci, A. A., Leboissetier, A., LeGrande, A. N., Lo, K. K., Marshall, J., Matthews, E. E.,
1062 McDermid, S., Mezzuman, K., Miller, R. L., Murray, L. T., Oinas, V., Orbe, C., García-Pando, C. P., Perlwitz, J. P., Puma, M.
1063 J., Rind, D., Romanou, A., Shindell, D. T., Sun, S., Tausnev, N., Tsigaridis, K., Tselioudis, G., Weng, E., Wu, J., and Yao,
1064 M.: GISS-E2.1: Configurations and Climatology, *J Adv Model Earth Syst*, 12, e2019MS002025,
1065 <https://doi.org/10.1029/2019MS002025>, 2020.

1066
1067 Kessler, W. S.: EOF Representations of the Madden–Julian Oscillation and Its Connection with ENSO, *J. Climate*, 14, 3055–
1068 3061, [https://doi.org/10.1175/1520-0442\(2001\)014<3055:EROTMJ>2.0.CO;2](https://doi.org/10.1175/1520-0442(2001)014<3055:EROTMJ>2.0.CO;2), 2001.

1069
1070 Kiladis, G. N., Wheeler, M. C., Haertel, P. T., Straub, K. H., and Roundy, P. E.: Convectively coupled equatorial waves,
1071 *Reviews of Geophysics*, 47, 2008RG000266, <https://doi.org/10.1029/2008RG000266>, 2009.

1072
1073 Kim, D., Xavier, P., Maloney, E., Wheeler, M., Waliser, D., Sperber, K., Hendon, H., Zhang, C., Neale, R., Hwang, Y.-T., and
1074 Liu, H.: Process-Oriented MJO Simulation Diagnostic: Moisture Sensitivity of Simulated Convection, *Journal of Climate*, 27,
1075 5379–5395, <https://doi.org/10.1175/JCLI-D-13-00497.1>, 2014.

1076
1077 Kim, H., Caron, J. M., Richter, J. H., and Simpson, I. R.: The Lack of QBO-MJO Connection in CMIP6 Models, *Geophysical
1078 Research Letters*, 47, e2020GL087295, <https://doi.org/10.1029/2020GL087295>, 2020.

1079
1080 Kim, J., K. M. Grise, and S.-W. Son, 2013: Thermal characteristics of the cold-point tropopause region in CMIP5 models,
1081 *Journal of Geophysical Research - Atmospheres*, 118, 8827–8841.

1082
1083 Klotzbach, P., Abhik, S., Hendon, H. H., Bell, M., Lucas, C., G. Marshall, A., and Oliver, E. C. J.: On the emerging relationship
1084 between the stratospheric Quasi-Biennial oscillation and the Madden-Julian oscillation, *Sci Rep*, 9, 2981,
1085 <https://doi.org/10.1038/s41598-019-40034-6>, 2019.

1086
1087 Kumar, V., Yoden, S., and Hitchman, M. H.: QBO and ENSO Effects on the Mean Meridional Circulation, Polar Vortex,
1088 Subtropical Westerly Jets, and Wave Patterns During Boreal Winter, *JGR Atmospheres*, 127,
1089 e2022JD036691, <https://doi.org/10.1029/2022JD036691>, 2022.

1090
1091 Lawrence, Z. D., Elsbury, D., Butler, A. H., Perlwitz, J., Albers, J. R., Ciasto, L. M., and Ray, E.: Evaluation of Processes
1092 Related to Stratosphere–Troposphere Coupling in GFSv12 Subseasonal Hindcasts, *Monthly Weather Review*, 151, 1735–
1093 1755, <https://doi.org/10.1175/MWR-D-22-0283.1>, 2023.

Deleted: Kawatani, Y., Hamilton, K., Watanabe, S., M., Taguchi, Serva, F., Anstey, J. A., Richter, J. H., Butchart, N., Orbe, C., Osprey, S. M., Naoe, H., Elsbury, D., Chen, C.-C., García-Serrano, J., Glanville, A., Kerzenmacher, T., Lott, F., Palmeiro, F. M., Park, M., Versick, S., and Yoshida, K.: QBO El Niño Southern Oscillation experiments Part I: Overview of experiment design and ENSO modulation of the QBO, *Weather and Climate Dynamics* (in press

Deleted:), <https://doi.org/10.5194/egusphere-2024-3270>, 2025.

1104 [Liebmann, B., and Smith, C. A.:](#) Description of a Complete (Interpolated) Outgoing Longwave Radiation Dataset, *Bulletin of*
1105 *the American Meteorological Society* 77, 6, 1274–78. <https://doi.org/10.1175/1520-0477-77.6.1274>, 1996.

1106

1107 [Lim, Y. and Son, S.:](#) QBO-MJO Connection in CMIP5 Models, *JGR Atmospheres*, 125, e2019JD032157,
1108 <https://doi.org/10.1029/2019JD032157>, 2020.

1109

1110 [Lin, H.:](#) The Madden-Julian Oscillation, *Atmosphere-Ocean*, 60, 338–359, <https://doi.org/10.1080/07055900.2022.2072267>,
1111 2022.

1112

1113 [Madden, R. A. and Julian, P. R.:](#) Observations of the 40–50-Day Tropical Oscillation—A Review, *Mon. Wea. Rev.*, 122, 814–
1114 837, [https://doi.org/10.1175/1520-0493\(1994\)122<0814:OOTDIO>2.0.CO;2](https://doi.org/10.1175/1520-0493(1994)122<0814:OOTDIO>2.0.CO;2), 1994.

1115

1116 [Martin, Z., S.-W. Son, A. Butler, H. Hendon, H. Kim, A. Sobel, S. Yoden, and C. Zhang, 2021:](#) The influence of the Quasi-
1117 Biennial Oscillation on the Madden-Julian Oscillation, *Nature Reviews Earth & Environment*, [https://doi.org/10.1038/s43017-](https://doi.org/10.1038/s43017-021-00173-9)
1118 021-00173-9.

1119

1120 [Martin, Z. K., Simpson, I. R., Lin, P., Orbe, C., Tang, Q., Caron, J. M., Chen, C., Kim, H., Leung, L. R., Richter, J. H., and](#)
1121 [Xie, S.:](#) The Lack of a QBO-MJO Connection in Climate Models With a Nudged Stratosphere, *JGR Atmospheres*, 128,
1122 e2023JD038722, <https://doi.org/10.1029/2023JD038722>, 2023.

1123

1124 [Matsuno, T.:](#) Quasi-Geostrophic Motions in the Equatorial Area, *Journal of the Meteorological Society of Japan*, 44, 25–43,
1125 https://doi.org/10.2151/jmsj1965.44.1_25, 1966.

1126

1127 [Miura, H., Maeda, T., and Kimoto, M.:](#) A Comparison of the Madden-Julian Oscillation Simulated by Different Versions of
1128 the MIROC Climate Model, *SOLA*, 8, 165–169, <https://doi.org/10.2151/sola.2012-040>, 2012.

1129

1130 [Nakamura, Y. and Takayabu, Y. N.:](#) Convective Couplings with Equatorial Rossby Waves and Equatorial Kelvin Waves. Part
1131 I: Coupled Wave Structures, *Journal of the Atmospheric Sciences*, 79, 247–262, <https://doi.org/10.1175/JAS-D-21-0080.1>,
1132 2022.

1133

1134 [Naoe, H., García-Franco, J. L., Park, C.-H., Rodrigo, M., Palmeiro, F. M., Serva, F., Taguchi, M., Yoshida, K., Anstey, J. A.,](#)
1135 [García-Serrano, J., Son, S.-W., Kawatani, Y., Butchart, N., Hamilton, K., Chen, C.-C., Glanville, A., Kerzenmacher, T., Lott,](#)
1136 [F., Orbe, C., Osprey, S., Park, M., Richter, J. H., Versick, S., and Watanabe, S.:](#) QBOi El Niño–Southern Oscillation
1137 experiments: teleconnections of the QBO, *Weather Clim. Dynam.*, 6, 1419–1442, [https://doi.org/10.5194/wcd-6-1419-2025-](https://doi.org/10.5194/wcd-6-1419-2025-2025)
1138 2025.

1139

1140 [Newman, M., Sardeshmukh, P. D., and Penland, C.:](#) How Important Is Air–Sea Coupling in ENSO and MJO Evolution?,
1141 *Journal of Climate*, 22, 2958–2977, <https://doi.org/10.1175/2008JCLI2659.1>, 2009.

1142

1143 [Nordeng, T.-E.:](#) Extended versions of the convective parametrization scheme at ECMWF and their impact on the mean and
1144 transient activity of the model in the tropics, <https://doi.org/10.21957/E34XWHYSW>, 1994.

1145

1146 [Orbe, C., Van Roekel, L., Adames, Á. F., Dezfúli, A., Fasullo, J., Gleckler, P. J., Lee, J., Li, W., Nazarenko, L., Schmidt, G.](#)
1147 [A., Sperber, K. R., & Zhao, M.:](#) Representation of Modes of Variability in Six U.S. Climate Models, *Journal of Climate*,
1148 33(17), 7591–7617. <https://doi.org/10.1175/JCLI-D-19-0956.1>, 2020.

1149

1150 [Pahlavan, H. A., Wallace, J. M., Fu, Q., and Kiladis, G. N.:](#) Revisiting the Quasi-Biennial Oscillation as Seen in ERA5. Part
1151 II: Evaluation of Waves and Wave Forcing, *Journal of the Atmospheric Sciences*, 78, 693–707, [https://doi.org/10.1175/JAS-](https://doi.org/10.1175/JAS-D-20-0249.1)
1152 D-20-0249.1, 2021.

1153

Commented [FS64]: the BAMS archiving is messed up!

Deleted: Naoe, H., García-Franco, J. L., Park, C.-H., Rodrigo, M., Palmeiro, F. M., Serva, F., Taguchi, M., Yoshida, K., Anstey, J. A., García-Serrano, J., Son, S.-W., Kawatani, Y., Butchart, N., Hamilton, K., Chen, C.-C., Glanville, A., Kerzenmacher, T., Lott, F., Orbe, C., Osprey, S., Park, M., Richter, J. H., Versick, S., and Watanabe, S.: QBOi El Niño Southern Oscillation experiments: Teleconnections of the QBO, *EGUsphere* [preprint

Deleted:], <https://doi.org/10.5194/egusphere-2025-1148>, 2025.

Commented [FS66]: if we keep the related sentence

1164 Pan, D. and Randall, D. D. A.: A cumulus parameterization with a prognostic closure, *Quart J Royal Meteor Soc*, 124, 949–
1165 981, <https://doi.org/10.1002/qj.49712454714>, 1998.
1166
1167 Pang, B., Chen, Z., Wen, Z., and Lu, R.: Impacts of two types of El Niño on the MJO during boreal winter, *Adv. Atmos. Sci.*,
1168 33, 979–986, <https://doi.org/10.1007/s00376-016-5272-2>, 2016.
1169
1170 Pascoe, C. L., Gray, L. J., Crooks, S. A., Juckes, M. N., and Baldwin, M. P.: The quasi-biennial oscillation: Analysis using
1171 ERA-40 data, *J. Geophys. Res.*, 110, 2004JD004941, <https://doi.org/10.1029/2004JD004941>, 2005.
1172
1173 Philander, S. G.: *El Niño, La Niña, and the southern oscillation*, Academic Press, San Diego, 293 pp., 1990.
1174
1175 Pohl, B. and Matthews, A. J.: Observed Changes in the Lifetime and Amplitude of the Madden–Julian Oscillation Associated
1176 with Interannual ENSO Sea Surface Temperature Anomalies, *Journal of Climate*, 20, 2659–2674,
1177 <https://doi.org/10.1175/JCLI4230.1>, 2007.
1178
1179 Puy, M., Vialard, J., Lengaigne, M., and Guilyardi, E.: Modulation of equatorial Pacific westerly/easterly wind events by the
1180 Madden–Julian oscillation and convectively-coupled Rossby waves, *Clim Dyn*, 46, 2155–2178,
1181 <https://doi.org/10.1007/s00382-015-2695-x>, 2016.
1182
1183 Randall, D. A., Tziperman, E., Branson, M. D., Richter, J. H., and Kang, W.: The QBO–MJO Connection: A Possible Role
1184 for the SST and ENSO, *Journal of Climate*, 36, 6515–6531, <https://doi.org/10.1175/JCLI-D-23-0031.1>, 2023.
1185
1186 Richter, J. H., Anstey, J. A., Butchart, N., Kawatani, Y., Meehl, G. A., Osprey, S., and Simpson, I. R.: Progress in Simulating
1187 the Quasi-Biennial Oscillation in CMIP Models, *JGR Atmospheres*, 125, e2019JD032362,
1188 <https://doi.org/10.1029/2019JD032362>, 2020.
1189
1190 Rind, D., Jonas, J., Balachandran, N. K., Schmidt, G. A., and Lean, J.: The QBO in two GISS global climate models: 1.
1191 Generation of the QBO, *JGR Atmospheres*, 119, 8798–8824, <https://doi.org/10.1002/2014JD021678>, 2014.
1192
1193 Rind, D., Orbe, C., Jonas, J., Nazarenko, L., Zhou, T., Kelley, M., Lacis, A., Shindell, D., Faluvegi, G., Romanou, A., Russell,
1194 G., Tausnev, N., Bauer, M., and Schmidt, G.: GISS Model E2.2: A Climate Model Optimized for the Middle Atmosphere—
1195 Model Structure, Climatology, Variability, and Climate Sensitivity, *JGR Atmospheres*, 125, e2019JD032204,
1196 <https://doi.org/10.1029/2019JD032204>, 2020.
1197
1198 Roundy, P. E.: The Spectrum of Convectively Coupled Kelvin Waves and the Madden–Julian Oscillation in Regions of Low-
1199 Level Easterly and Westerly Background Flow, *Journal of the Atmospheric Sciences*, 69, 2107–2111,
1200 <https://doi.org/10.1175/JAS-D-12-060.1>, 2012.
1201
1202 Sakaeda, N., Dias, J., and Kiladis, G. N.: The Unique Characteristics and Potential Mechanisms of the MJO–QBO Relationship,
1203 *JGR Atmospheres*, 125, e2020JD033196, <https://doi.org/10.1029/2020JD033196>, 2020.
1204
1205 Schenzinger, V., Osprey, S., Gray, L., and Butchart, N.: Defining metrics of the Quasi-Biennial Oscillation in global climate
1206 models, *Geosci. Model Dev.*, 10, 2157–2168, <https://doi.org/10.5194/gmd-10-2157-2017>, 2017.
1207
1208 Schreck, C. J.: Global Survey of the MJO and Extreme Precipitation, *Geophysical Research Letters*, 48,
1209 e2021GL094691, <https://doi.org/10.1029/2021GL094691>, 2021.
1210
1211 Serva, F., Anstey, J. A., Bushell, A. C., Butchart, N., Cagnazzo, C., Gray, L. J., Kawatani, Y., Osprey, S. M., Richter, J. H.,
1212 and Simpson, I. R.: The impact of the QBO on the region of the tropical tropopause in QBOi models: Present-day simulations,
1213 *Quart J Royal Meteor Soc*, 148, 1945–1964, <https://doi.org/10.1002/qj.4287>, 2022.

1214
1215 Serva, F., Christiansen, B., Davini, P., Von Hardenberg, J., Van Den Oord, G., Reerink, T. J., Wyser, K., and Yang, S.: Changes
1216 in Stratospheric Dynamics Simulated by the EC-Earth Model From CMIP5 to CMIP6, *J Adv Model Earth Syst*, 16,
1217 e2023MS003756, <https://doi.org/10.1029/2023MS003756>, 2024.

1218
1219 Slingo, J. M., Rowell, D. P., Sperber, K. R., and Nortley, F.: On the predictability of the interannual behaviour of the Madden-
1220 Julian oscillation and its relationship with el Niño, *Quart J Royal Meteor Soc*, 125, 583–609,
1221 <https://doi.org/10.1002/qj.49712555411>, 1999.

1222
1223 Son, S.-W., Lim, Y., Yoo, C., Hendon, H. H., and Kim, J.: Stratospheric Control of the Madden–Julian Oscillation, *Journal of*
1224 *Climate*, 30, 1909–1922, <https://doi.org/10.1175/JCLI-D-16-0620.1>, 2017.

1225
1226 Straub, K. H. and Kiladis, G. N.: Observations of a Convectively Coupled Kelvin Wave in the Eastern Pacific ITCZ, *J. Atmos.*
1227 *Sci.*, 59, 30–53, [https://doi.org/10.1175/1520-0469\(2002\)059<0030:OOACCK>2.0.CO;2](https://doi.org/10.1175/1520-0469(2002)059<0030:OOACCK>2.0.CO;2), 2002.

1228
1229 Suematsu, T. and Miura, H.: Zonal SST Difference as a Potential Environmental Factor Supporting the Longevity of the
1230 Madden–Julian Oscillation, *Journal of Climate*, 31, 7549–7564, <https://doi.org/10.1175/JCLI-D-17-0822.1>, 2018.

1231
1232 Suematsu, T. and Miura, H.: Changes in the Eastward Movement Speed of the Madden–Julian Oscillation with Fluctuation in
1233 the Walker Circulation, *Journal of Climate*, 35, 211–225, <https://doi.org/10.1175/JCLI-D-21-0269.1>, 2022.

1234
1235 Sun, L., Wang, H., and Liu, F.: Combined effect of the QBO and ENSO on the MJO, *Atmospheric and Oceanic Science*
1236 *Letters*, 12, 170–176, <https://doi.org/10.1080/16742834.2019.1588064>, 2019.

1237
1238 Tam, C.-Y. and Lau, N.-C.: Modulation of the Madden-Julian Oscillation by ENSO: Inferences from Observations and GCM
1239 Simulations, *Journal of the Meteorological Society of Japan*, 83, 727–743, <https://doi.org/10.2151/jmsj.83.727>, 2005.

1240
1241 Tegtmeier, S., Anstey, J., Davis, S., Ivanciu, I., Jia, Y., McPhee, D., and Pilch Kedzierski, R.: Zonal Asymmetry of the QBO
1242 Temperature Signal in the Tropical Tropopause Region, *Geophysical Research Letters*, 47, e2020GL089533,
1243 <https://doi.org/10.1029/2020GL089533>, 2020.

1244
1245 Tiedtke, M.: A Comprehensive Mass Flux Scheme for Cumulus Parameterization in Large-Scale Models, *Mon. Wea. Rev.*,
1246 117, 1779–1800, [https://doi.org/10.1175/1520-0493\(1989\)117<1779:ACMFSF>2.0.CO;2](https://doi.org/10.1175/1520-0493(1989)117<1779:ACMFSF>2.0.CO;2), 1989.

1247
1248 Vitart, F.: Madden—Julian Oscillation prediction and teleconnections in the S2S database, *Quart J Royal Meteor Soc*, 143,
1249 2210–2220, <https://doi.org/10.1002/qj.3079>, 2017.

1250
1251 Waliser, D., Sperber, K., Hendon, H., Kim, D., Maloney, E., Wheeler, M., Weickmann, K., Zhang, C., Donner, L., Gottschalck,
1252 J. and Higgins, W. MJO simulation diagnostics. *J. Climate*, 22, 3006–3030, <https://doi.org/10.1175/2008JCLI2731.1>, 2009

1253
1254 Wang, B., Chen, G., and Liu, F.: Diversity of the Madden-Julian Oscillation, *Sci. Adv.*, 5, eaax0220,
1255 <https://doi.org/10.1126/sciadv.aax0220>, 2019.

1256
1257 Wang, T. and Li, T.: Diversity of MJO Initiation Regions and Processes, *Journal of Climate*, 35, 3121–3140,
1258 <https://doi.org/10.1175/JCLI-D-21-0816.1>, 2022.

1259
1260 Wang, Y.-C., Tseng, W.-L., and Hsu, H.-H.: Role of convection–circulation coupling in the propagation mechanism of the
1261 Madden–Julian Oscillation over the Maritime Continent in a climate model, *Clim Dyn*, 58, 2469–2484,
1262 <https://doi.org/10.1007/s00382-021-06013-2>, 2022.

1263

Commented [FS67]: Is the new Wang 2017 missing?

Commented [de68R67]: i deleted it

1264 Wei, Y. and Ren, H.-L.: Modulation of ENSO on Fast and Slow MJO Modes during Boreal Winter, *Journal of Climate*, 32,
1265 7483–7506, <https://doi.org/10.1175/JCLI-D-19-0013.1>, 2019.

1266

1267 Wheeler, M. C. and Hendon, H. H.: An All-Season Real-Time Multivariate MJO Index: Development of an Index for
1268 Monitoring and Prediction, *Mon. Wea. Rev.*, 132, 1917–1932, [https://doi.org/10.1175/1520-0493\(2004\)132<1917:AARMMI>2.0.CO;2](https://doi.org/10.1175/1520-0493(2004)132<1917:AARMMI>2.0.CO;2), 2004.

1269

1270 Yadav, P. and Straus, D. M.: Circulation Response to Fast and Slow MJO Episodes, *Monthly Weather Review*, 145, 1577–
1272 1596, <https://doi.org/10.1175/MWR-D-16-0352.1>, 2017.

1273

1274 [Yadav, P., Garfinkel, C. I., and Domeisen, D. I. V.: The Role of the Stratosphere in Teleconnections Arising From Fast and
1275 Slow MJO Episodes, *Geophysical Research Letters*, 51, e2023GL104826, <https://doi.org/10.1029/2023GL104826>, 2024.

1276

1277 [Yang, G.-Y. and Hoskins, B. J.: ENSO impact on Kelvin waves and associated tropical convection, *J. Atmos. Sci.*, 70, 3513–3532, <https://doi.org/10.1175/JAS-D-13-081.1>, 2013.](https://doi.org/10.1175/JAS-D-13-081.1)

1278

1279 [Yang, G.-Y. and Hoskins, B. J.: ENSO-related variation of equatorial MRG and Rossby waves and forcing from higher latitudes, *Quart. J. Roy. Meteor. Soc.*, 142, 2488–2504, <https://doi.org/10.1002/qj.2842>, 2016.](https://doi.org/10.1002/qj.2842)

1280

1281 [Yang, G.-Y., Feng, X., and Hodges, K.: Seasonal and interannual variation of equatorial waves in ERA5 and GloSea5, *Quart. J. Roy. Meteor. Soc.*, 149, 1109–1134, <https://doi.org/10.1002/qj.4460>, 2023.](https://doi.org/10.1002/qj.4460)

1282

1283

1284

1285

1286 Yoo, C., and S.-W. Son, 2016: Modulation of the boreal wintertime Madden-Julian Oscillation by the stratospheric Quasi-Biennial Oscillation, *Geophysical Research Letters*, 43, 1392-1398.

1287

1288

1289 Yukimoto, S., Kawai, H., Koshiro, T., Oshima, N., Yoshida, K., Urakawa, S., Tsujino, H., Deushi, M., Tanaka, T., Hosaka, M., Yabu, S., Yoshimura, H., Shindo, E., Mizuta, R., Obata, A., Adachi, Y., and Ishii, M.: The Meteorological Research Institute Earth System Model Version 2.0, MRI-ESM2.0: Description and Basic Evaluation of the Physical Component, *Journal of the Meteorological Society of Japan*, 97, 931–965, <https://doi.org/10.2151/jmsj.2019-051>, 2019.

1290

1291

1292

1293

1294 Yuni, A. R. E., Lubis, S. W., and Setiawan, S.: Vertical structure of Convectively Coupled Equatorial Waves (CCEWs) during Boreal Summer and Winter, *IOP Conf. Ser.: Earth Environ. Sci.*, 284, 012010, <https://doi.org/10.1088/1755-1315/284/1/012010>, 2019.

1295

1296

1297

1298 Zhang, C. and Gottschalck, J.: SST Anomalies of ENSO and the Madden–Julian Oscillation in the Equatorial Pacific*, *J. Climate*, 15, 2429–2445, [https://doi.org/10.1175/1520-0442\(2002\)015<2429:SAOEAT>2.0.CO;2](https://doi.org/10.1175/1520-0442(2002)015<2429:SAOEAT>2.0.CO;2), 2002.

1299

1300

1301 Zhang, G. J. and McFarlane, N. A.: Sensitivity of climate simulations to the parameterization of cumulus convection in the Canadian climate centre general circulation model, *Atmosphere-Ocean*, 33, 407–446, <https://doi.org/10.1080/07055900.1995.9649539>, 1995.

1302

1303

1304

1305 Zhu, J., Kumar, A., and Wang, W.: Dependence of MJO Predictability on Convective Parameterizations, *Journal of Climate*, 33, 4739–4750, <https://doi.org/10.1175/JCLI-D-18-0552.1>, 2020.

1306

1307

1308

Commented [FS69]: Next, the three Yang's papers should be added

